LAWRENCE
LIVERMORE
NATIONAL
LABORATORY

LLNL-JRNL-807522

Process Modeling and Techno-Economic Analysis of a CO2 Capture Process Using Fixed Bed Reactors with a Microencapsulated Solvent

G. Kotamreddy, R. Hughes, D. Bhattacharyya, J. Stolaroff, K. Hornbostel, M. Matuszewski, B. Omell

March 23, 2020

Energy & Fuels

Disclaimer

Process Modeling and Techno-Economic Analysis of Fixed Bed Reactors for CO_2 Capture using a Microencapsulated Solvent

Goutham Kotamreddy[1], Ryan Hughes[1], Debangsu Bhattacharyya[1], Joshua Stolaroff[2], Katherine Hornbostel[3], Michael Matuszewski[4], Benjamin Omell[4]

[1]Department of Chemical and Biomedical Engineering, West Virginia University, Morgantown, WV 26506, USA

[2]Lawrence Livermore National Laboratory, Livermore, CA 94551, USA

[3]Department of Mechanical Engineering and Materials Science, University of Pittsburgh, Pittsburgh, PA 15261, USA

[4] National Energy Technology Laboratory, 626 Cochrans Mill Rd, Pittsburgh, PA 15236, USA

Abstract

A detailed model of a capsule containing sodium carbonate solution is developed here to study the microencapsulated carbon capture solvents (MECS). A rigorous vapor-liquid equilibrium (VLE) model is developed for the Na_2CO_3-CO_2-H_2O system, where liquid phase nonideality is modeled by the electrolyte non-random two-liquid (eNRTL) model. The data from the experiments conducted at Lawrence Livermore National Laboratory (LLNL) is used to obtain a maximum likelihood estimate of the initial solvent concentration inside the capsules and the parameters present in the capsule model. A non-isothermal, dynamic model of a fixed bed contactor filled with these capsules is then developed. In addition to direct steam injection, indirect heating using an embedded heat exchanger is modeled for desorption. Finally, the model is used to simulate temperature swing absorption and desorption cycles. The results of these studies indicate that there is an optimal residence time or superficial flue gas velocity to minimize the bed volume. However, the total energy requirement for desorption monotonically decreases with increased residence time as the proportion of the sensible heat to the total regeneration heat keeps decreasing. Furthermore, heat recovery from the bed is crucial to keep energy penalty for regeneration low. A techno-economic analysis is conducted and equivalent annual operating cost (EAOC) is analyzed for two different reactor materials (concrete and carbon-steel) and compared with a system using a conventional MEA solvent. The minimum EAOC for the MECS fixed bed configuration is approximately 1.8-2.7 times higher than the EAOC for an MEA system with similar amount of heat recovery (85%). The impact of +/-50% uncertainty in capital cost estimate is also evaluated and the minimum EAOC is 1.5 times higher than MEA technology for 85% heat recovery. These results using microencapsulated sodium carbonate solution are a starting point that sets an upper limit on cost for MECS carbon capture system. Reasonable improvements to the MECS capsules (e.g. using a higher carbonate concentration, using a faster-acting solvent like an ionic liquid) and also exploring other contactor technologies should all lower system cost and make it more competitive with amine systems.

Key Words

Microencapsulated carbon capture solvents (MECS), Fixed bed reactor, Sodium carbonate solution, CO_2 capture, Techno-economic analysis

---

* Corresponding author.
Tel:1-304-293-9335, E-mail: Debangsu.Bhattacharyya@mail.wvu.edu

1. INTRODUCTION

Many strategies have been proposed to mitigate greenhouse gas emissions such as switching to less carbon-intensive fuels, using renewable energy sources, and improving the efficiency of energy conversion devices [Metz et al. 2005]. Carbon capture and storage is one of the key strategies in combating climate change because power production using fossil fuel is projected to continue as a major power source in the foreseeable future [EIA 2019]. Several advanced technologies are being developed for CO_2 capture because the state-of-the-art monoethanolamine (MEA) based carbon capture technology has several drawbacks such as corrosion, energy penalty. [Nielsen et al., 2012; Reynolds et al., 2012].

Microencapsulation of liquid sorbents is new, promising technology for the capture of carbon dioxide that could overcome the challenges associated with MEA [Vericella et al., 2015]. Microencapsulation is a microfluidic process where a substance is encapsulated within an inert polymer material. The microcapsules containing the solvent can be produced with diameters ranging from 100-600 microns. The small size of these microcapsules results in a high specific surface area per unit volume, which enhances mass and thermal transport 100-fold. Carbon capture solvents that absorb CO_2 slower than MEA in a typical tower can now absorb CO_2 faster than MEA (per unit reactor volume) if they're encapsulated. Motivations behind encapsulation of a substance can widely vary. Immobilization of volatile material, release of a substance in a controlled manner over a period of time, and managing phase separation are a few of the motivations. Microencapsulation can also be applied to process engineering applications that require handling of solids/slurry or highly viscous materials, bypassing operational issues such as clogging of equipment, high pumping cost, and lack of homogeneity in the process fluids.

The use of carbonate solutions to absorb CO_2, known as the Benfield process, has been widely studied [Benson et al., 1954; Pinsent et al., 1956; Savage et al., 1980; Astarita et al., 1981; Pohorecki et al., 1990; Kohl 1997; Knnutila et al., 2010]. Carbonate solutions offer many advantages such as easy regeneration, low solvent cost, and low toxicity. However, carbonate solutions for CO_2 absorption have been overlooked in the past due to their slower kinetics and solids formation. Microencapsulation of carbonate solution can help in overcoming these issues. Vericella et al. (2015) at Lawrence Livermore National Laboratory (LLNL) first demonstrated microencapsulated carbonate solution for carbon capture The same team at LLNL then showed carbon capture using ionic liquids [Stolaroff et al. 2016]. More recently, the LLNL team demonstrated that a variety of capsules (including carbonates with and without catalysts) could absorb CO_2 effectively over 10 absorption/desorption cycles [Knipe et al., 2019]. These studies have focused primarily on experimental demonstration of MECS. However, a couple of recent papers have dealt with modeling MECS filled with sodium carbonate solution. One group at the National Energy Technology Laboratory developed a detailed model of a single carbonate capsule to study the absorption reaction and

water flux across the shell [Finn et al., 2018]. The Lawrence Livermore group [Hornbostel et al., 2019] developed a simplified carbonate capsule model to estimate the sizes and energy penalties of both fixed bed and fluidized bed absorbers. Hornbostel et al., 2019 used an empirical model for the Na_2CO_3-CO_2-H_2O reaction to predict the CO_2 absorption rate in the presence of cyclen catalyst. The authors assumed isothermal conditions in the fixed bed reactor, which may not be possible considering the CO_2 absorption and water movement between the flue gas and capsules. Hornbostel et al. also made simplifying assumptions about the regeneration process (e.g. assuming a constant heat of reaction, fixing the regeneration time at 10 minutes) due to a lack of experimental data on the regeneration process. The authors also did not account for water flux across the capsule shell, which is a critical aspect of carbonate capsule performance. However, detailed modeling of fixed bed reactors for MECS and techno-economic analysis (TEA) of these systems for CO_2 capture is lacking in the current literature.

The present work adds onto the MECS reactor modeling performed by Hornbostel et al. 2019 by including detailed reactions, water flux, and temperature variation in order to accurately resolve the performance of carbonate MECS in a fixed bed reactor. The purpose of this modeling work is to evaluate the commercial feasibility of MECS in a fixed bed configuration for CO_2 capture. Therefore, a techno-economic analysis (TEA) is performed here for a range of materials and operating parameters, and the results are compared to the state-of-the-art MEA carbon capture technology. Raksajati et al. (2017), performed a TEA on both fixed and fluidized beds of MECS filled with MEA instead of carbonate solution. That group made some simplifying assumptions, e.g. lumping mass transfer resistances and assuming uniform loading throughout the fixed bed. These assumptions may be reasonable for MEA capsules, but they would break down for carbonate capsules, which absorb CO_2 slowly. Therefore, detailed mass transfer and heat transfer models are incorporated into our TEA work to study the performance of carbonate capsules.

In this paper, a detailed multi-scale model of a fixed bed reactor filled with sodium carbonate capsules is developed. The microcapsule model presented in section 3 encompasses reaction kinetics, a rigorous VLE model, and mass transfer resistances. The reactor scale model simulating both absorption and regeneration stages for a temperature swing system is also presented in section 3. The parameter estimation approach discussed in section 4 is used to obtain a maximum likelihood estimate of the mass transfer model parameters. Finally, a cost model of this system for the TEA is presented in Section 5. The validation with experimental data, modeling and TEA results are presented and discussed (Section 6) and then conclusions are drawn (Section 7).

2. EXPERIMENTAL SYSTEM

Figure 1 shows the schematic of the experimental setup used to study the CO_2 absorption using encapsulated carbonate solvent. The experimental data obtained from this setup is used to estimate parameters corresponding to the mass transfer model. The capsules are spread as a single layer on top of a mesh tray and placed in the reaction chamber. A pool of water is placed to achieve 100% humidity in the chamber. Before the start of the experiment, the ball valve is turned to vacuum pump to reach a minimum pressure value (~0.15 psi). Then, the vacuum pump is shutoff and the ball valve turned to CO_2 to release a fixed amount into the chamber. As the microcapsules start to absorb CO_2, the decrease in the gas pressure with respect to time is noted. More details about the experimental setup can be found in Vericella et al. [2015]. The size of the microcapsules and the reaction chamber are provided in the Table1.

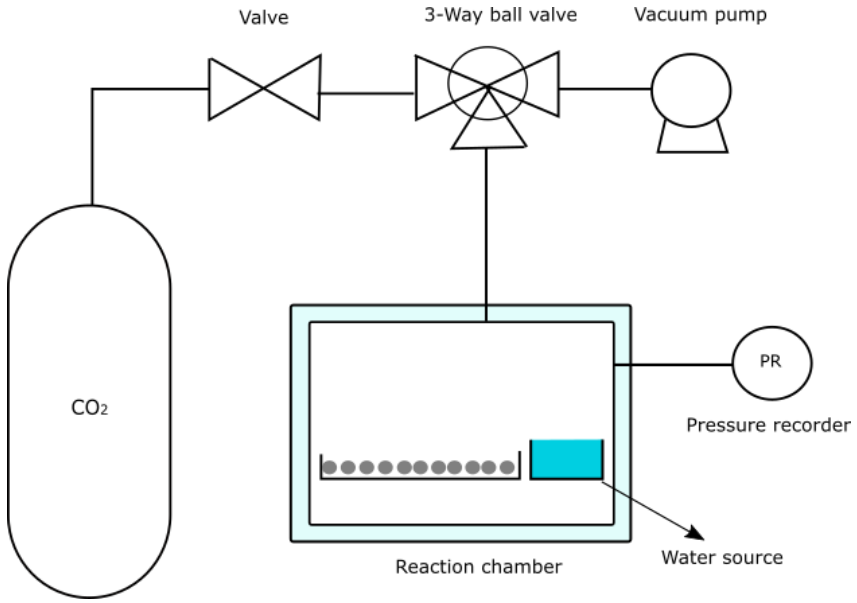

Figure 1. Experimental setup of CO_2 absorption using microcapsules filled with sodium carbonate.

Table 1. Dimensions of the microcapsules and volume of the chamber

Variable Name	Symbol	Value	Units
Capsule radius	R_{cap}	3e-4	m
Core radius	R_c	2.63e-4	m
Reaction chamber volume	V_R	4.5e-5	m^3

3. MODEL DEVELOPMENT

3.1. Reaction model. In the system studied here, the encapsulated solvent is sodium carbonate and the shell is made of polydimethylsiloxane (PDMS). The overall reaction of CO_2 in the sodium carbonate solution is

$$CO_2 + H_2O + Na_2CO_3 \leftrightarrow 2NaHCO_3 \quad (1)$$

The main reactions involved in the absorption of CO_2 using Na_2CO_3 solution are as follows [Astarita et al., 1981, Knuutila et al., 2010]

$$CO_2 + OH^- \leftrightarrow HCO_3^- \quad (2)$$

$$CO_3^{2-} + H_2O \leftrightarrow HCO_3^- + OH^- \quad (3)$$

The rate controlling step for this system is reaction (2). Reaction (3) is considered to be instantaneous. The chemistry can be described using the following reactions

$$2H_2O \leftrightarrow H_3O^+ + OH^- \quad (4)$$

$$CO_2 + 2H_2O \leftrightarrow HCO_3^- + H_3O^+ \quad (5)$$

$$HCO_3^- + H_2O \leftrightarrow CO_3^{2-} + H_3O^+ \quad (6)$$

As the sodium carbonate is a strong electrolyte, it is assumed to be completely dissociated in the water to form sodium and carbonate ions.

$$Na_2CO_3 \leftrightarrow 2Na^+ + CO_3^{2-} \quad (7)$$

Equilibrium constants for the above reactions and the rate constants are obtained from the literature [Edwards et al., 1978; Pinsent et al., 1956]. The eNRTL model in AspenPlus® is used to represent the thermodynamics of this system using model parameters from the literature [Knuutila et al., 2010].

The liquid molar enthalpy in the eNRTL model is calculated using solvent enthalpy, electrolyte enthalpy at infinite dilution, and excess molar enthalpy which is defined as

$$H_L = x_w h_w^o + \sum_k x_k h_k^{\infty,aq} + h^{*ex} \quad (8)$$

where *w* is water and *k* denotes electrolyte species. The solvent enthalpy is defined as

$$h_w^o = \Delta_f h_w^{ig} + \int_{298.15}^{T} c_{p,w}^{ig} dT + \left(h_w(T,P) - h_w^{ig}(T,P)\right) \quad (9)$$

The molar enthalpy of electrolyte species at infinite dilution is given as

$$h_k^{\infty,aq} = \Delta_f h_k^{\infty,aq} + \int_{298.15}^{T} c_{p,k}^{\infty,aq} dT \tag{10}$$

The molar excess enthalpy can be calculated using

$$h^{*ex} = -RT^2 \sum_i x_i \frac{\partial ln\gamma_i}{\partial T} \tag{11}$$

where R is the gas constant. The elementary balance for all the species present in the Na_2CO_3-CO_2-H_2O system can be written as

$$C_{Na_2CO_3,core} + C_{CO_2,core} = C^*_{CO_2,core} + C^*_{Na_2CO_3,core} + C_{HCO_3^-,core} + C_{CO_3^{2-},core} \tag{12}$$

$$C_{H_2O,core} = C^*_{H_2O,core} + C_{HCO_3^-,core} + C_{OH^-,core} + C_{H_3O^+,core} \tag{13}$$

$$C_{Na_2CO_3,core} = C^*_{Na_2CO_3,core} + 0.5C_{Na^+,core} \tag{14}$$

$$C_{Na^+,core} + C_{H_3O^+,core} = 2C_{CO_3^{2-},core} + C_{OH^-,core} + C_{HCO_3^-,core} \tag{15}$$

The equilibrium relationship for the reactions (4-6) are given by:

$$K_w = \frac{[C_{H_3O^+,core}][C_{OH^-,core}]}{[C^2_{H_2O,core}]} \tag{16}$$

$$K_{eq1} = \frac{[C_{HCO_3^-,core}][C_{H_3O^+,core}]}{[CO^*_{2,core}][C_{H_2O,core}]^2} \tag{17}$$

$$K_{eq2} = \frac{[C_{CO_3^{2-},core}][C_{H_3O^+,core}]}{[C_{HCO_3^-,core}][C_{H_2O,core}]} \tag{18}$$

The vapor-liquid equilibrium for CO_2 and H_2O at the shell/core interface is described using

$$\phi_{CO_2} P y_{CO_2,int} = He_{CO_2} \gamma_{CO_2} x_{CO_2,int} \tag{19}$$

$$\phi_{H_2O} P y_{H_2O,int} = x_{H_2O,int} \gamma_{H_2O} f^L_{H_2O} \tag{20}$$

The fugacity coefficients for CO_2 and H_2O are obtained using SRK model while the activity coefficients are obtained using the eNRTL model as noted earlier. Henry's law constants for sodium carbonate solutions are obtained from the literature [Knuutila et al., 2010].

3.2. Model of a single microcapsule. The fundamental heat and mass transfer mechanisms in developing a reactor scale model differs in comparison to the microcapsule level model. The different mechanisms occurring at a microcapsule level are captured with the help of a single microcapsule model. The microcapsule in this study is modeled as two distinct components, solvent as the core and a solid polymer encapsulating the solvent. Figure 2 shows the schematic of a single microcapsule. The following assumptions are made while developing the capsule model: (1) all capsules are perfectly spherical, (2)

there is no accumulation within the shell wall, (3) the core fluid is well mixed, (4) mass transfer through the shell is only through diffusion, and (5) there is no loss of the solvent through the membrane.

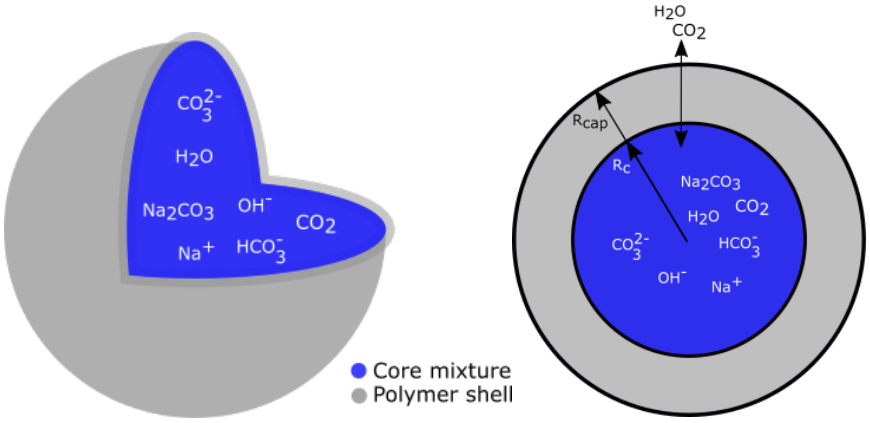

Figure 2. Schematic of microcapsule showing shell and core components.

Species continuity equation for the components diffusing through the shell can be written as:

$$\frac{1}{r^2}\frac{\partial}{\partial r}\left(D_{i,shell}\, r^2 \frac{\partial C_{i,shell}}{\partial r}\right) = 0 \tag{21}$$

where the boundary conditions at the shell surface (R_{cap}) and at the interface of core liquid (R_c) and shell are given by:

$$D_{i,shell}\frac{\partial C_{i,shell}}{\partial r} = N_{i,G} \tag{22}$$

$$D_{i,shell}\frac{\partial C_{i,shell}}{\partial r} = N_{i,L} \tag{23}$$

The corresponding equations for both the fluxes are given as

$$N_{i,G} = k_{i,G}(C_{i,G} - C_{i,shell}) \tag{24}$$

$$N_{i,L} = E k_{i,L} C_{T,L}(x_{i,int} - x_i^*) \tag{25}$$

The enhancement factor (E) is given by the equation

$$E = Ha = \frac{\sqrt{k_1 C_{OH^-} D_{CO_2,L}}}{k_{CO_2,L}} \tag{26}$$

The component balance for the core liquid is given by

$$\frac{d(C_{CO_2,core})}{dt} = a_e\, N_{CO_2,L} \tag{27}$$

$$\frac{d(C_{H_2O,core})}{dt} = a_e\, N_{H_2O,L} \tag{28}$$

$$\frac{d(C_{Na_2CO_3,core})}{dt} = 0 \tag{29}$$

The overall balance on the liquid core is written as

$$C_{T,L} = \sum C_{i,core} \tag{30}$$

The shell energy balance is written as:

$$\rho_{shell} C_{p,shell} \frac{\partial T_s}{\partial t} = K_{shell}\left(\frac{2}{r}\frac{\partial T_s}{\partial r} + \frac{\partial^2 T_s}{\partial r^2}\right) \tag{31}$$

The core energy balance is written as

$$\frac{\partial (C_{T,L} H_L)}{\partial t} = h_c a_e (T_s - T_c) + a_e N_{CO_2,L} \bar{H}_{CO_2,L} + a_e N_{H_2O,L} \Delta H_{vap} \tag{32}$$

Corresponding boundary conditions are given by

$$-K_{shell}\frac{\partial T_s}{\partial r} = h_C (T_c - T_s) \tag{33}$$

$$-K_{shell}\frac{\partial T_s}{\partial r} = h_{gs} (T_s - T_g) \tag{34}$$

3.3. Model of the experimental system. In the experimental system described in Section 2, mass transfer takes place from the stationary gas to the static capsules. The following correlations are used for the liquid and gas phase mass transfer coefficients [Cussler 1997; Kumar et.al. 1999] for a static spherical particle. The CO_2 diffusion coefficient through the polymer shell is estimated using the experimental data.

$$\frac{k_{i,L} d_{core}}{D_{i,L}} = \frac{2\pi^2}{3} \tag{35}$$

$$\frac{k_{i,G} d_{cap}}{D_{i,G}} = 2 + 0.6\left(\frac{d_{cap}^3 \Delta\rho g}{\rho_G \mu_G^2}\right)^{\frac{1}{4}}\left(\frac{\mu_G}{D_{i,G}}\right)^{\frac{1}{3}} \tag{36}$$

The overall mass balance equation for the gas phase present in the experimental reactor described earlier is given by

$$\frac{dC_{Gbulk,R}}{dt} = -\frac{n_{cap}\left(N_{surf} A_{cap}\right)}{V_R} \tag{37}$$

where $C_{Gbulk,R}$ is the total gas phase concentration in the reaction chamber V_R.

3.4. Modeling of a fixed bed reactor. The reactor configuration explored in this modeling study is a fixed bed temperature swing absorption with the combination of both direct and indirect heating approach as shown in the Figure 3. The direct heating approach, where a hot stream is directly injected into the bed, is widely used for temperature swing adsorption. Since a CO_2-rich stream is desired for sequestration, typically steam is injected as it can be easily condensed from the stream exiting the desorber. However, since steam cannot be condensed in a fixed bed system containing MECS, only the sensible heat from the steam is available for heating thus a large amount of steam will be needed to regenerate the encapsulated chemical solvent, if the entire amount of heat has to be provided by the injected steam.

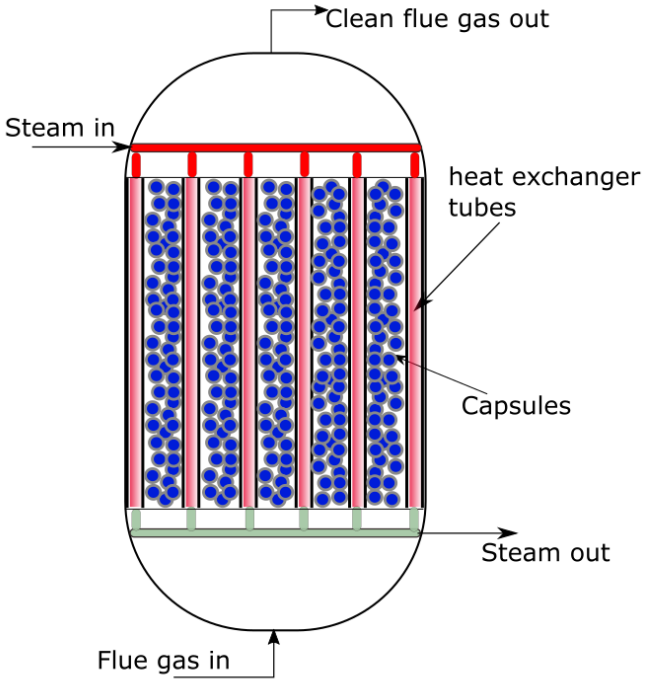

Figure 3. Schematic of fixed bed configuration for MECS showing capsules, heat exchanger tubes and flow directions.

The indirect heating approach, where the heat is provided by an embedded heat exchanger through which steam or some other hot utility can be sent, can be helpful in solving the issues mentioned above [Bonjour et al., 2002; Clausse et al., 2010; Duarte et al., 2016]. However, the direct injection of the steam has the advantage that other than heating, it also reduces the partial pressure of CO_2 in the system thus reducing the temperature required to regenerate the solvent to a certain loading. Furthermore, due to the presence of steam, water loss from the solvent inside the capsule can be greatly reduced. Therefore both direct heating through injection of steam to the bed as well as indirect heating by condensing steam in an embedded heat exchanger are considered.

The fixed bed model developed here has three phases- the gas phase that enters into the fixed bed as feed, the solid phase constituting the polymer shell, and the liquid phase i.e., the absorbing liquid present inside the polymer shell. The assumptions made in the modeling of the fixed bed are: (1) the gas behavior is assumed to follow SRK equation of state, (2) only axial variation of the transport variables corresponding to the bulk phase is considered, (3) pressure drop follows the Ergun equation, (4) the embedded heat exchanger is assumed to have a triangular pitch arrangement for the tubes.. The heat and mass transfer correlations along with boundary conditions used in the model are provided in the supporting information.

Mass balance

Gas Phase

$$\epsilon_{bed}\frac{\partial C_{i,G}}{\partial t} = -\frac{\partial\left(u_G C_{i,G}\right)}{\partial z} - (1-\epsilon_{bed})a_{e,cap}N_{i,G} \tag{38}$$

Energy balance

Gas Phase

$$\begin{aligned}\epsilon_{bed}\frac{\partial(C_{T,G}H_G)}{\partial t} = &-\frac{\partial(u_G C_{T,G}H_G)}{\partial z} - (1-\epsilon_{bed})a_{e,cap}\left(N_{CO_2,G}\overline{H}_{CO_2,G} + N_{H_2O,G}\overline{H}_{H_2O,G}\right)\\ &- (1-\epsilon_{bed})a_{e,cap}h_{gs}\left(T_g - T_s\right) + a_{e,hx}\,h_{hxwG}\left(T_{hxw} - T_g\right)\end{aligned} \tag{39}$$

Heat exchanger tube wall

$$\rho_{hxw}\,C_{p,hxw}\frac{\partial T_{hxw}}{\partial t} = a_{e,hx}h_{hxw}(T_{sat} - T_{hxw}) - a_{e,hx}h_{hxwG}\left(T_{hxw} - T_g\right) + K_{hxw}\frac{\partial^2 T_{hxw}}{\partial z^2} \tag{40}$$

Pressure Drop (Ergun Equation)

$$\frac{\partial P}{\partial z} = -\left\{\frac{150\mu_g(1-\varepsilon_{bed})^2}{d_{cap}^2\varepsilon_{bed}^3}u_G + \frac{1.75\rho_g(1-\varepsilon_{bed})}{d_{cap}\varepsilon_{bed}^3}u_G^2\right\} \tag{41}$$

4. PARAMETER ESTIMATION AND DATA RECONCILIATION APPROACH

The diffusivity parameter in the mass transfer model, $D_{i,shell}$ in eq. (21) needs to be estimated. The parameter $D_{i,shell}$ is given by

$$D_{i,shell} = C_{i,1}\exp\left(-\frac{C_{i,2}}{T}\right) \tag{42}$$

Furthermore, even though a good guess of the initial solvent concentration in the microcapsule, $C_{Na_2CO_3,core}\big|_{t=0}$, is available, an exact value at the beginning of the experiment is not available as the concentration of the encapsulated solvent is practically impossible to measure and therefore should be reconciled. The log-likelihood objective function considered for parameter estimation is

$$\max_{C_1,C_2,C_{Na_2CO_3,core}|_{t=0}} \left\{ -\frac{1}{2} \sum_{i=1}^{Nmeas} \left(n_i \log(2\pi + 1) + n_i \log \left[\frac{1}{n_i} \sum_{j=1}^{NDyn} \sum_{k=1}^{M_{ij}} w_j^2 \frac{\left(Z_e(t_{ijk}) - Z_m(t_{ijk})\right)^2}{Z_{m,ijk}^{\gamma_i}} \right] + \theta_i \sum_{j=1}^{NDyn} \sum_{k=1}^{M_{ij}} \log w_j \, Z(t_{ijk}) \right) \right\}$$

The number of unique variables that are measured over all experiments is denoted as $Nmeas$. The term $w_j^2 \frac{\left(Z_e(t_{ijk}) - Z_m(t_{ijk})\right)^2}{Z_{m,ijk}^{\gamma_i}}$ is the weighted modeling error calculated for all the dynamic experiments, in which Z_m denotes the value of the measured variable, and Z_e represents the corresponding value calculated from the model. The term θ_i is a heteroscedasticity parameter that is used to account for the standard error of the observations. This value is automatically calculated during the maximization of the log likelihood function.

5. COST MODEL

The capital cost is estimated for two different materials of construction- carbon steel and concrete. The capital cost for carbon steel as material of construction is obtained using Aspen Process Economic Analyzer (APEA®). The fixed bed configuration has an embedded heat exchanger which is represented in APEA® as a shell and tube heat exchanger to calculate the capital cost. However, the size of the exchanger is larger than the maximum size available in APEA®. Therefore, the purchased cost is first obtained from the APEA® for the maximum size of the heat exchanger. Then the cost of the heat exchanger corresponding to the actual embedded heat exchanger is calculated using Eq. (43). Finally, the bare module cost is calculated from the purchased cost by applying the correlations from Turton et al. (2018).

$$Esimated\ cost = Base\ cost \left(\frac{required\ area}{base\ area} \right)^{0.6} \tag{43}$$

The capital cost for the contactor made from concrete is performed using some internal information that includes material, direct and indirect costs which are shown in the Table 2. The internal wall-to-floor area and roof area are used in the capacity scaling to find the capital cost of a single bed is done by applying Eq. (43). The cost of heat exchanger tubes embedded in the concrete exchanger is calculated using APEA®. The cost of the capsules including the solvent and the shell material is calculated using internal data as shown in Table 2. The cost of the low pressure process steam is taken from Turton et al. (2018) to calculate the operating cost.

Table 2. Unit prices used in the capital cost estimation of concrete and capsules

	Cost	Basis	Source
Concrete	2174 ($/m^2)	Internal wall to floor area	(Rochelle, 2018)
Capsule	0.0593 ($/kg)	Mass of capsules	(Stolaroff, 2018)

The inlet flue gas is compressed to meet the pressure drop requirements of the fixed bed reactor. The capital cost for the compressors is obtained using APEA®. The operating cost required for the compressors is calculated using the power needed to achieve the required compression. The equivalent annual operating cost (EAOC) is calculated by adding the annualized capital cost to the yearly operating cost (YOC) [Turton et al., 2018] using Eq. (44). The annualized capital cost is obtained by amortizing the total capital cost over the period of plant life. The discount rate is assumed to be 10% and the operating life for the reactors and compressors, is assumed to be 10 years and 2 years for the capsules. The TEA of the MECS system is compared with that of conventional MEA-based CO_2 capture in towers. For the MEA system, capital and operating costs are obtained from Case 11B in the National Energy Technology Laboratory (NETL) baseline study [Fout et al., 2015].

$$EAOC = Capital\ cost \frac{i}{(1-(1+i)^{-n})} + YOC \tag{44}$$

Where i is the discount rate and n is the number of operating years.

6. RESULTS AND DISCUSSION

6.1. VLE model validation. The VLE model developed for Na_2CO_3-CO_2-H_2O system presented in Section 3 is validated with the limited data available in the open literature [Knuutila et al., 2010]. Figure 4 compares the model results with the experimental data for 10 wt% solvent at 40ºC and 80ºC. Figure 4 shows the change in CO_2 loading with increase in the partial pressure of CO_2. The model can be further improved by obtaining the data at lower CO_2 loadings, high sodium carbonate concentrations, and for a wider temperature range.

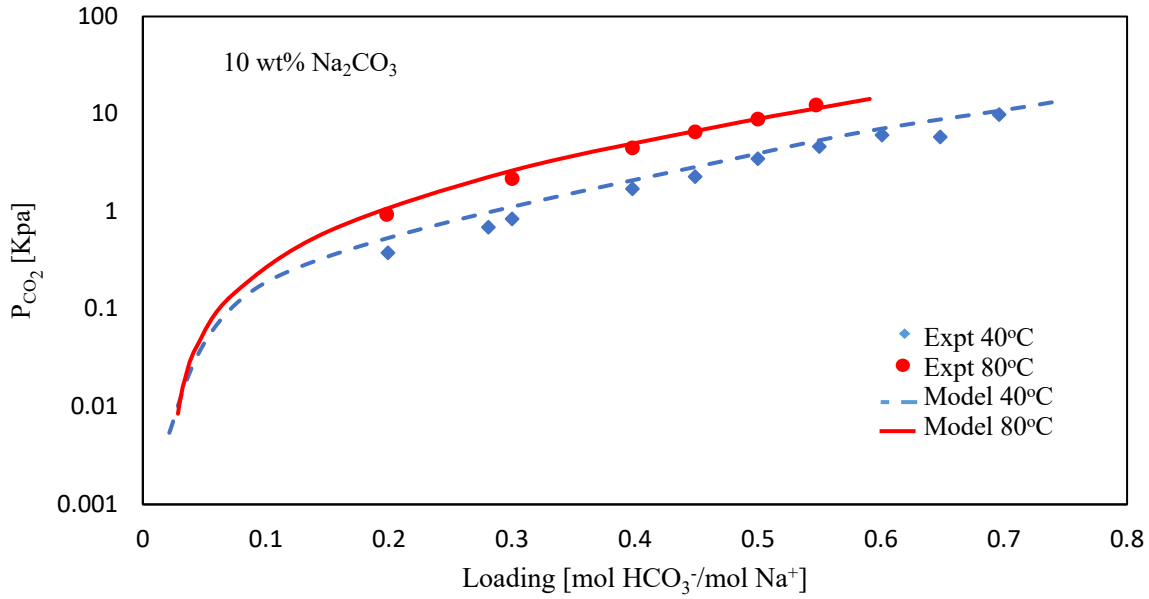

Figure 4. VLE model validation for 10 wt% Na_2CO_3 capsules.

6.2. Heat of absorption. The heat of absorption data for Na_2CO_3-CO_2-H_2O system is scarce in the literature. The authors could find only one value for heat of absorption at 25°C reported by Berg et al., 1978. The heat of absorption as a function of temperature and CO_2 loading is calculated using the enthalpy model presented in Section 3.1. Gao et al., 2015 reported the heat of absorption for K_2CO_3 solvent system. The heat of absorption trend shown in the Figure 5 agrees qualitatively with potassium carbonate solvent reported by Gao et al.

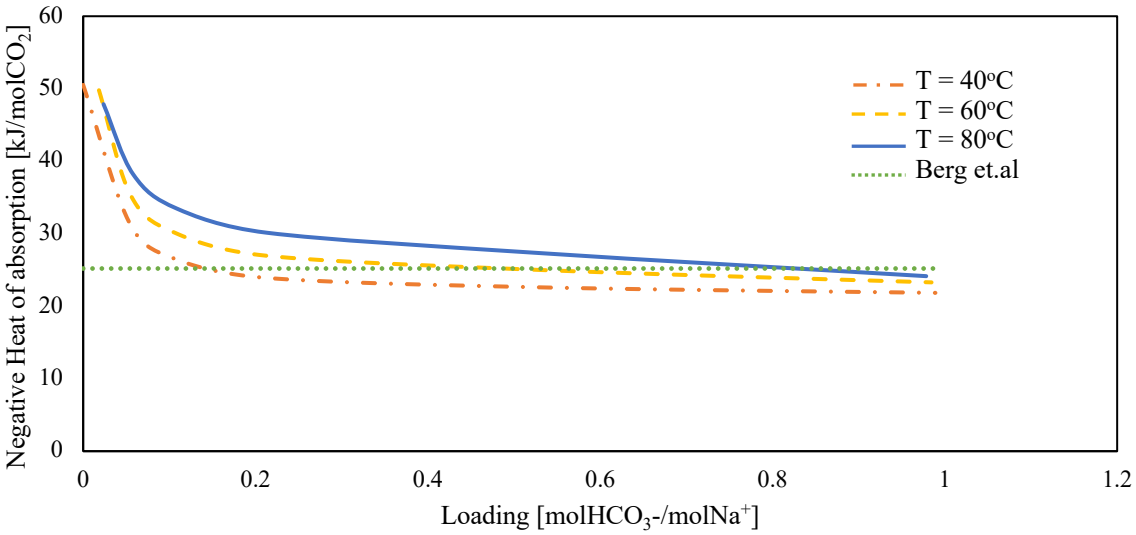

Figure 5. Heat of absorption for 10 wt% Na_2CO_3 solution.

It can be seen from the figure using a constant value underestimates the heat of absorption at lower loadings and overestimates at higher loadings. Therefore, capturing the nonlinearity in the heat of absorption is critical especially for contactors like fixed beds where there is considerable temporal and/or spatial variation of CO_2 loading.

6.3. Parameter estimation, data reconciliation, and model validation. As mentioned in the section 4, the CO_2 diffusivity parameters within the PDMS shell wall are estimated. The initial solvent concentration in microcapsules presents an uncertainty about the state of core solvent inside the shell. Table 3 presents the estimated parameters and reconciled initial solvent concentration along with their corresponding lower and upper bounds. The microcapsule model is validated using the estimated parameters and reconciled initial solvent concentration against the experimental data. Figure 6 compares the model results for the transients in the total gas pressure with the experimental data at 25°C, 40°C, and 60°C. It can be seen that the model results match very well with the experimental data.

Table 3. Estimated model parameters and reconciled variables

Temperature	Parameter/Variable	Estimated/ reconciled value	Lower bound	Upper bound	Units	Std. deviation	Initial value
	C_1	2.153e-8	1e-8	1e-5	[m^2/s]	4.6e-10	2.5e-8
	C_2	1106	1000	2500	[K]	6.7	1200
25°C	Solvent	7.8	5	12	wt%	0.003	10
40°C	concentration	7.6	5	12	wt%	0.002	10
60°C		6.2	5	12	wt%	0.002	10

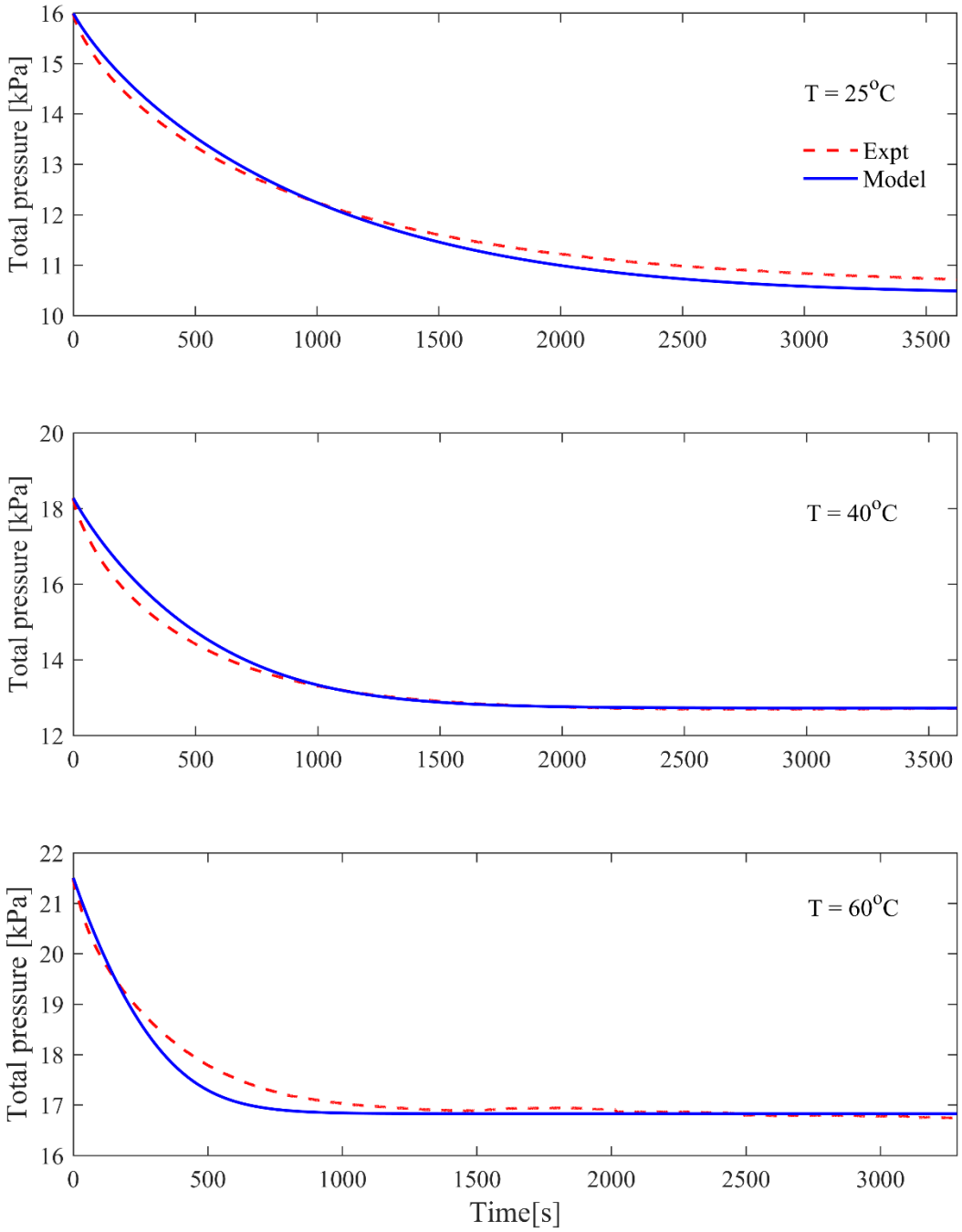

Figure 6. Comparison between the model results and the experimental data for the transients in the reactor chamber pressure at 25°C, 40°C, and 60°C.

6.4. Impact of key design and operating variables. The impact of major operating variables on regeneration energy and economics of the MECS have been investigated. The variables examined are the flue gas residence time, initial bed temperature, heat recovery, and reaction rate. The absorption rate of CO_2 in the carbonate solutions can be enhanced using a catalyst. In all the studies presented here, the capsules are considered to be filled with sodium carbonate solution without any catalyst unless specified otherwise. The techno- economic analysis on MECS is performed considering two different materials of construction for fixed bed reactor. The results of the study are compared to standard MEA technology.

6.4.1. Impact of residence time. One of the key design variables for fixed beds is the residence time of reactants in a bed, which is a function of the bed diameter, height, and the flowrate through it. A higher residence time can help to obtain higher volume-averaged loading that is closer to the equilibrium loading. A higher residence time will also results in longer breakthrough time and lower energy penalty. These two aspects are analyzed in detail later. However, since the bed height is limited because of pressure drop constraints, a higher residence time can only be obtained by decreasing the flowrate or increasing the bed diameter, or by both. It should be noted that decreasing flowrate would lead to higher number of beds in parallel to process the total amount of the flue gas from the power plant. Thus, any of the options noted above will lead to a larger total cross-sectional area, which leads to higher total reactor volume and therefore higher capital cost. Therefore, the tradeoffs between the capital costs and operating costs need to be investigated to obtain the optimal residence time.

While the parameters for the diffusivity of CO_2 through the shell could be obtained by using the experimental data as noted earlier, we currently do not have in-house mass transfer data for H_2O through the shell. The shell diffusivity parameters for water is taken from the open literature for poly (dimethylsiloxane) material [Watson et al., 1996]. For calculating the breakthrough time, it is important to define the term breakthrough time first. It is expected that for CO_2 capture applications, there would not be any target for achieving an instantaneous CO_2 capture, rather an integral capture target over a period of time. Also, for a fixed bed, as the bed is taken in line, there is practically no CO_2 slip from the bed for some time. Therefore if there is an overall target of 90% CO_2 capture, when the breakthrough takes place, the capture may be lower than 90%. With these considerations, the breakthrough time is defined in this work as the maximum allowable time at which the integral CO_2 slip (i.e. CO_2 slip from the time the bed comes on line for absorption to the breakthrough time) reaches 10% of the total adsorbate that has been fed to the fixed bed over that period of time. The breakthrough time (t_b) is calculated using the equation:

$$F_{in} z_{CO_2,in} 0.1 t_b = \int_{t_0}^{t_0+t_b} F_{out}\, z_{CO_2,out}\, dt \tag{45}$$

where F_{in} is total molar flow into the bed, $z_{CO_2,in}$,and $z_{CO_2,out}$ are the inlet and outlet mole fractions of CO_2. The breakthrough time (t_b) depends mainly on the solvent under consideration and on the residence time of flue gas in the reactor. The effect of residence time on the key characteristics of a fixed bed reactor such as absorption time (breakthrough time), regeneration time, and number of beds in the cycle is analyzed. Later, the sensitivity of capital and operating cost of the fixed bed reactor with respect to residence time is also presented. The important operating and design variables fixed in this analysis are listed in Table 4. The studies presented here correspond to Case 11B in the NETL baseline study [Fout et al., 2015]. The subcritical pulverized coal power plant in this case produces 644 MWe gross power. The flue gas entering into the fixed bed contactor is assumed to be saturated with water at the inlet temperature since the flue gas typically passes through a scrubber before entering the capture system.

Table 4. Key variables in the fixed bed operation

Absorption Stage	Value	UOM
Length of the bed	10	m
Diameter of the bed	15	m
Outlet gas pressure	1.0	bar
Solvent concentration	20	wt%
Desorption Stage		
Inlet steam temperature	130	^oC
Steam residence time	100	s
Specific area for indirect heating	117	m^2/m^3
Average loading at the end of cycle	0.1	mol HCO_3^-/mol Na^+

Table 5 shows the effect of residence time on the key variables such as the breakthrough time (or absorption time), desorption time and total number of beds required in the cycle when the initial bed temperature is 40^{o}C. Since the outgoing clean flue gas from the capture system goes to the stack, the outlet pressure from the bed is specified to be 1 bar. Therefore, as the operating conditions are changed, the bed inlet pressure changes depending on the pressure drop through the bed that is calculated by the Ergun equation as mentioned earlier. The total number of beds is determined by solving a scheduling problem that ensures the required number of parallel beds for absorption is always available. As expected, with the increase in residence time, i.e. decrease in the superficial velocity, the breakthrough time keeps increasing and the number of beds in parallel under absorption keeps increasing. Since higher breakthrough time indicates higher loading of the capsules, correspondingly it takes a longer time to regenerate the bed. When the absorption and desorption times are similar, the number of beds undergoing absorption is similar to the number of beds undergoing desorption as expected. On the other hand, when the breakthrough time is much shorter than desorption time, for example when τ is 75 s, the number of beds in absorption cycle is much less than the number of beds in desorption cycle. However, the number of beds undergoing desorption decreases as the breakthrough time increases.

Table 5. Impact of residence time on the number of beds and cycle times

Residence time (τ) (s)	Breakthrough time (t_b) (s)	Desorption time (s)	Absorption beds	Total beds in the cycle
75	922	3425	25	118
100	2765	4223	38	97
150	6723	4495	67	112
200	10362	4518	96	138

The breakthrough curves and capsule loadings are shown in Figures 7 and 8, respectively, at different sections of the bed for two different residence times of the flue gas. For a fair comparison, the initial CO_2 loading of the capsules is specified to be zero for the results shown in Figures 7 and 8. It can be observed in Figure 7 that the outlet concentration at the breakthrough time for the bed with higher residence time is higher than the bed with the lower residence time. The reason becomes clear by considering the definition of the breakthrough time given by Eq. (45), which is based on the integral CO_2 slip, and by comparing the exit concentration profiles corresponding to the higher and lower residence times. Figure 8 shows the loadings at different nodes along the length of the bed. The volume-averaged loading of capsules is more at the higher residence time.

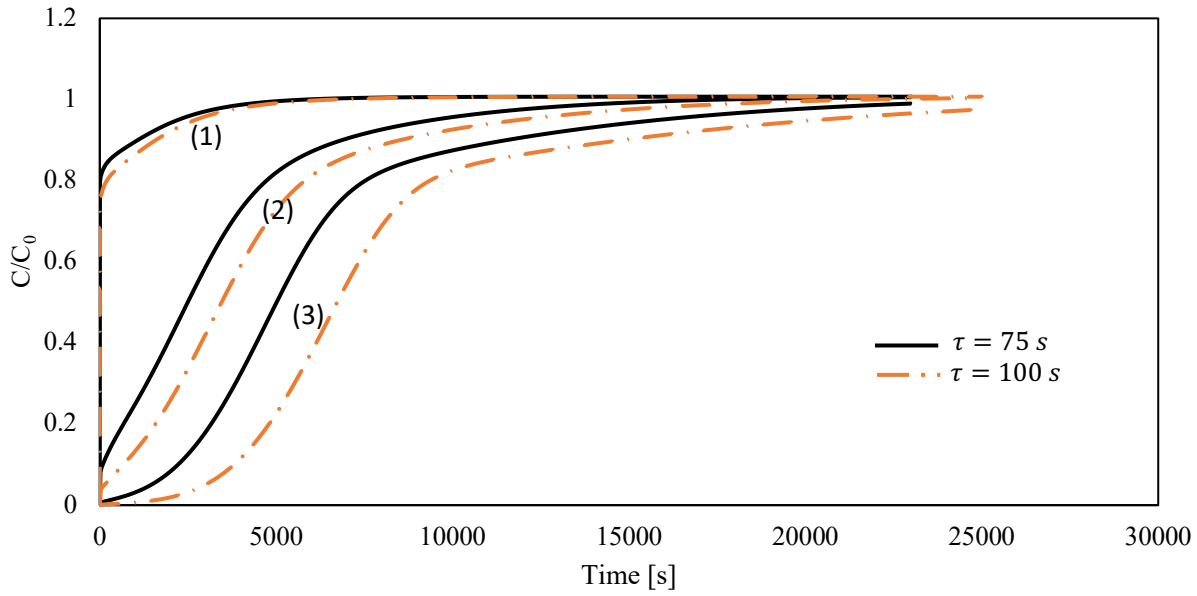

Figure 7. Breakthrough curve for different residence times at different locations: (1) entrance, (2) middle, (3) end of the bed.

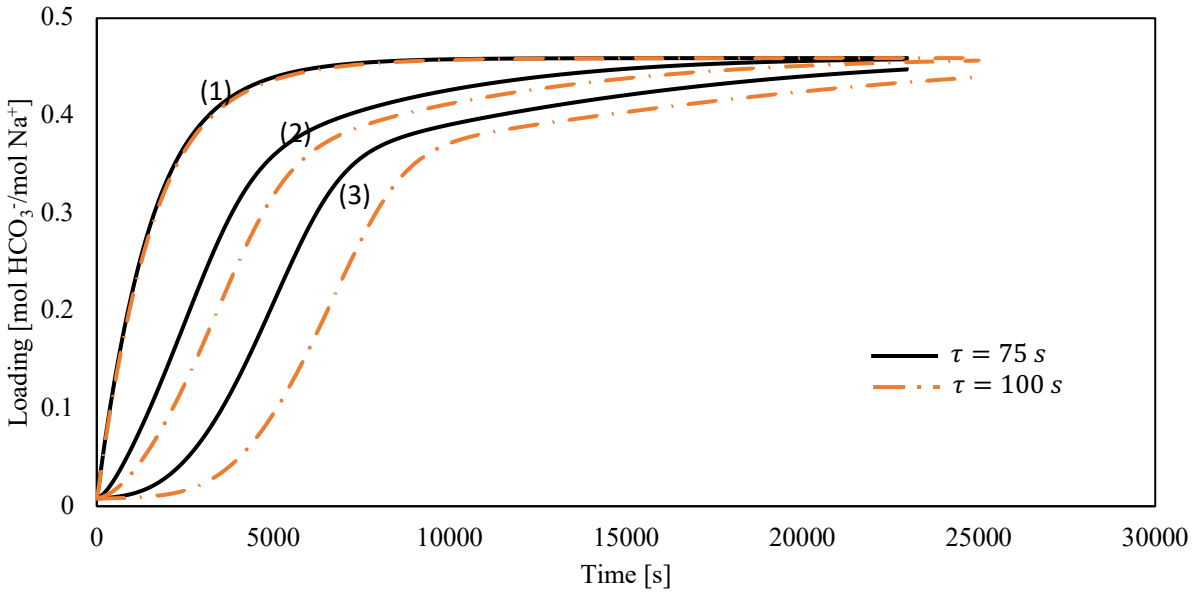

Figure 8. Loading comparison for different residence times at different locations: (1) entrance, (2) middle, (3) end of the bed.

This study shows that there is an optimum number of beds or minimum total volume of the bed corresponding to an optimal residence time. It should be noted that a decrease in the residence time or an increase in the superficial velocity results in an increase in the inlet pressure of the flue gas and the pressure drop through the bed as the outlet pressure remains fixed at 1 bar. Obviously, the maximum inlet pressure is observed for the lower residence time (high superficial velocity) and vice versa. When the operating range for superficial velocity varies from 42 s to 200 s, the inlet pressures change between 3.25 bar to 1.2 bar. The increase in the pressure helps to improve the loading, but at the cost of a blower, the capital and operating costs of which needs to be considered. Thus the optimization needs to be done with due consideration of the capital and operating costs of the entire system as presented later in this work.

6.4.2. Impact of initial bed temperature. An increase in the flue gas temperature and the bed temperature increases the rate of reaction but adversely affect the equilibrium CO_2 loadings. In addition, as the flue gas is saturated with water, a higher temperature leads to higher mass flowrate through the system leading to a decrease in the residence time. Figure 9 shows the sensitivity of the total bed volume for different initial bed temperatures. It is observed that when the residence time is lower, a higher bed temperature is advantageous due to the improvement of the reaction rate. However, as the residence time increases, the number of parallel beds undergoing absorption increases to a larger degree at higher temperatures when compared to the same residence time increase at lower temperature. This is due to the

higher mass flowrate as mentioned above thus leading to a steeper increase in the bed volume at higher temperature.

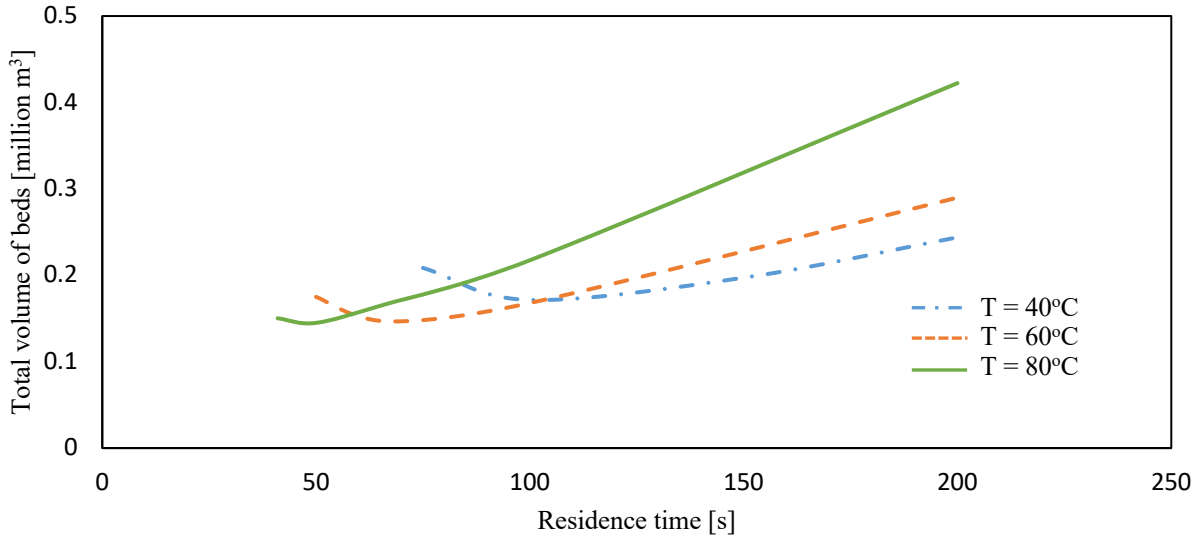

Figure 9. Impact of the residence time on the total volume of the beds at various initial bed temperatures.

The bed temperature also affects the regeneration duty. Figure 10 shows the effect of residence time on the regeneration duty for varying bed temperatures. The regeneration energy keeps monotonically decreasing with higher residence time as the sensible heat/total heat ratio keeps decreasing. An increase in absorption temperature reduces the temperature difference between absorption and desorption cycles, which, in turn, reduces the amount of sensible heat required for raising the temperature of the capsules and the solvent to the stripper temperature. However, the total volume of the beds undergoing regeneration must also be taken into consideration. It is observed that the regeneration energy requirement increases considerably if the bed temperature is at 40°C and residence time is less than about 100 s. For 40°C when the residence time decreases below 100 s, there is a substantial increase in the bed volume as shown in Fig.9. In addition, the relative difference in temperature between the absorption and desorption conditions is the highest for this case. These two effects result in a very high regeneration energy requirement. As the residence time increases, the regeneration energy requirement becomes lower for 40°C in comparison to 60°C and 80°C because of higher CO_2 loading at 40°C.

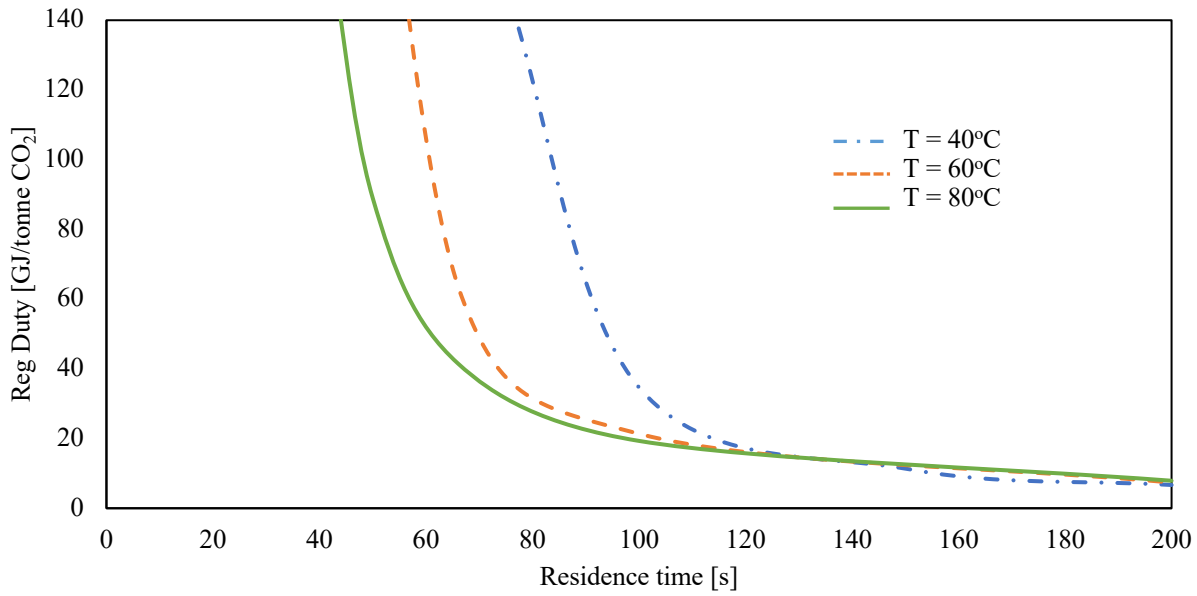

Figure 10. Impact of the residence time on the regeneration duty for various initial bed temperatures.

6.4.3. Impact of the reaction rate. The reaction of carbonate solutions with CO_2 is slow and can be promoted in the presence of a catalyst [Astarita et al., 1981, Nathalie et al., 2013]. Nathalie et al., 2013 studied the absorption of CO_2 in the aqueous sodium carbonate solution with and without carbonic anhydrase. The results showed that the presence of carbonic anhydrase catalyst in the carbonate solutions enhances the reaction rate of CO_2 with solvent approximately by 10 times. Therefore, the effect of reaction rate on the performance of fixed bed operation is analyzed. In the first case denoted as normal rate, the reaction rate is for an uncatalyzed solvent as presented before. In the other case here, denoted as '10 x normal rate', it is assumed that the catalyst can enhance the reaction rate by 10 times the 'normal rate' at all operating conditions. Regeneration duties along with other key parameters for both the cases and for both the residence times studied above are shown in Table 6. It can be noted that the case with larger residence time has lower energy requirement. The relative difference between the total volumes required for both residence times decreases as the reaction rate is increased. This analysis shows that the presence of a catalyst and a longer residence time i.e., a lower superficial velocity to the bed is beneficial. However, lower inlet superficial velocities increases the parallel number of beds operating in a cycle that leads to a higher capital cost. Therefore, one should consider a techno-economic analysis including both capital and operating costs in determining the optimum residence time. The results of such an analysis is presented in the ensuing sub-section.

Table 6. Key parameters showing energy and volume requirements for MECS in a fixed bed configuration

	Normal rate		10 x normal rate	
Variable	$\tau = 75\ s$	$\tau = 100\ s$	$\tau = 75\ s$	$\tau = 100\ s$
Absorption time	922	2765	2211	4053
Desorption time	3425	4223	4292	4432
Total beds in the cycle	118	97	74	80
Total Volume (m^3)	208523	171413	130768	141371
Regeneration duty (GJ/tCO_2)	150	35	36	17

6.4.4. Impact of heat recovery. The regeneration energy values shown in Table 6 are much higher than MEA which typically varies from 3.4-4.3 MJ/kg CO_2 [Knuutila et al., 2009]. Heat recovery can play a major role in reducing the overall energy penalty for regeneration. As mentioned earlier, the heat required during desorption stage can be delivered via two methods, direct heating and indirect heating. These methods can be provided alone or can be combined. Direct heating can be achieved by injecting steam into the bed. This method has the advantage that it also reduces the partial pressure of CO_2 thus a lower loading can be obtained even at a lower temperature. The main disadvantage is that since steam condensation external to the capsule is not desired, only very little heating duty can be obtained from the steam depending on the available superheat in the inlet steam and thus a large amount of steam will be required for providing the heat of desorption. Indirect heating is provided through steam condensation in an embedded heat exchanger. Indirect heating has the advantage of reduced steam consumption in comparison to direct heating. Its disadvantage is that a larger contactor size is needed due to the presence of the embedded heat exchanger. If only indirect heating is considered, CO_2 partial pressure in the bed will be high leading to a higher regeneration temperature than direct heating for a given desired loading from the regeneration cycle. Therefore, the likely optimal configuration will be a combination of direct and indirect heating methods to exploit the advantage of each of the methods. During absorption, the flue gas flow direction is downward. Obviously, at the time of breakthrough, the bed loading keeps decreasing from the top towards the bottom. During desorption, if the steam flow direction is downward, then as CO_2 concentration in the outgoing gas keeps increasing on the flow direction, CO_2 can get reabsorbed in the downstream capsules that have lower loading. To circumvent this issue, the flow direction during desorption is considered opposite to the flow direction during absorption.

In a conventional stripper for MEA, the sensible heat recovered from the liquid outlet stream for about 5°C temperature approach using a cross heat exchanger is about 80-90%. Raksajati et al. (2017) assumed 60% of total sensible heat duty can be recovered in their fixed bed studies for microencapsulation of MEA. This is based on the process scheme used in the dehydration unit of a natural gas processing plant. Figure 11

shows the variation of total regeneration duty with residence time for different extents of heat recovery for initial bed temperature of 40°C. The number of beds at any point undergoing desorption decreases and at the same time, the amount of CO_2 absorbed by the microcapsules increases with the increase in residence time. Overall, this reduces the total regeneration energy with the increase in the residence time as shown in Figure 11. It can be observed in Figure 11 that the heat recovery and residence time plays an important role to make the regeneration duty comparable to the MEA.

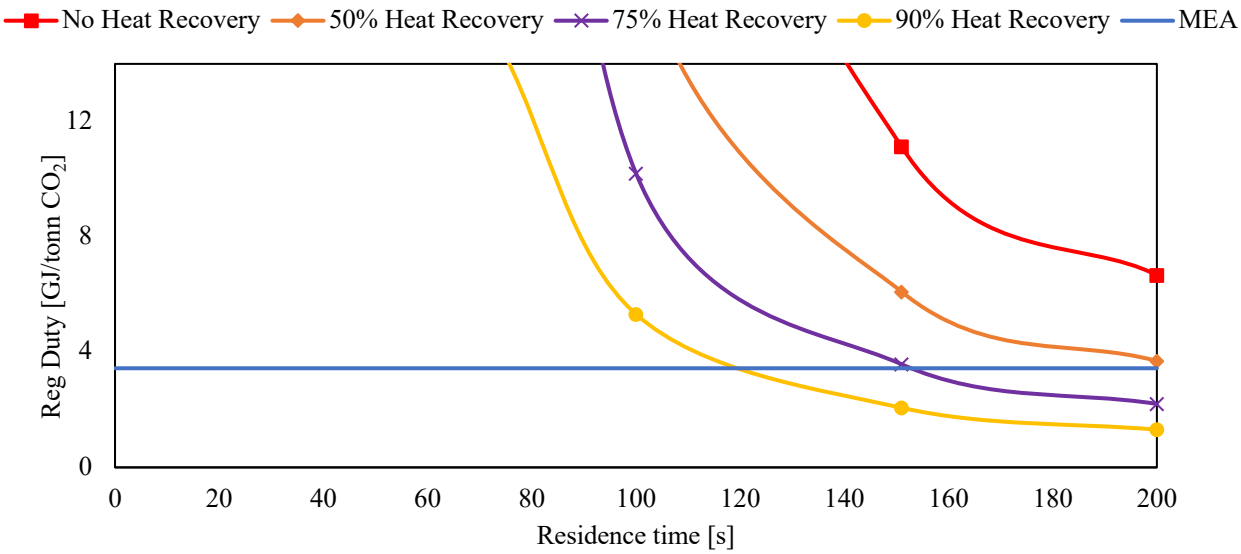

Figure 11. Impact of the residence time on regeneration duty for different extents of heat recovery.

6.5. Techno-economic studies. The studies presented in the earlier sections point to various design parameters and operating conditions that can improve the economics of the MECS system, but also show the strong tradeoff between the capital and operating costs as those design parameters and operating conditions are varied. Therefore a techno-economic study is undertaken. Equivalent annual operating cost (EAOC) is considered as the economic measure for this study. Two different materials of construction, carbon-steel and concrete, are considered for the absorber/desorber.

6.5.1. Impact of residence time and initial bed temperature. The impact of the residence time on the capital cost is analyzed for three different initial bed temperatures, 40°C, 60°C, and 80°C. As shown in Table 5, the number of beds goes through a minimum with increase in residence time. But, the regeneration energy keeps decreasing as shown in Figures 10 and 11. Figures 12 and 13 shows the annualized capital cost for concrete and carbon-steel respectively. The steeper increase in the annualized capital cost for the

initial bed temperature of 80°C is expected since Figure 9 shows the steep increase in the bed volume with the residence time for the initial bed temperature of 80°C and the capital cost is positively correlated to the bed volume. Figures 12 and 13 also show the annualized capital cost for the MEA system using packed absorber and strippers, which is found to be considerably lower than the MECS system operating with carbonate solvent in a fixed bed reactor. The capital cost for concrete based reactor is lower compared to reactor made using carbon-steel.

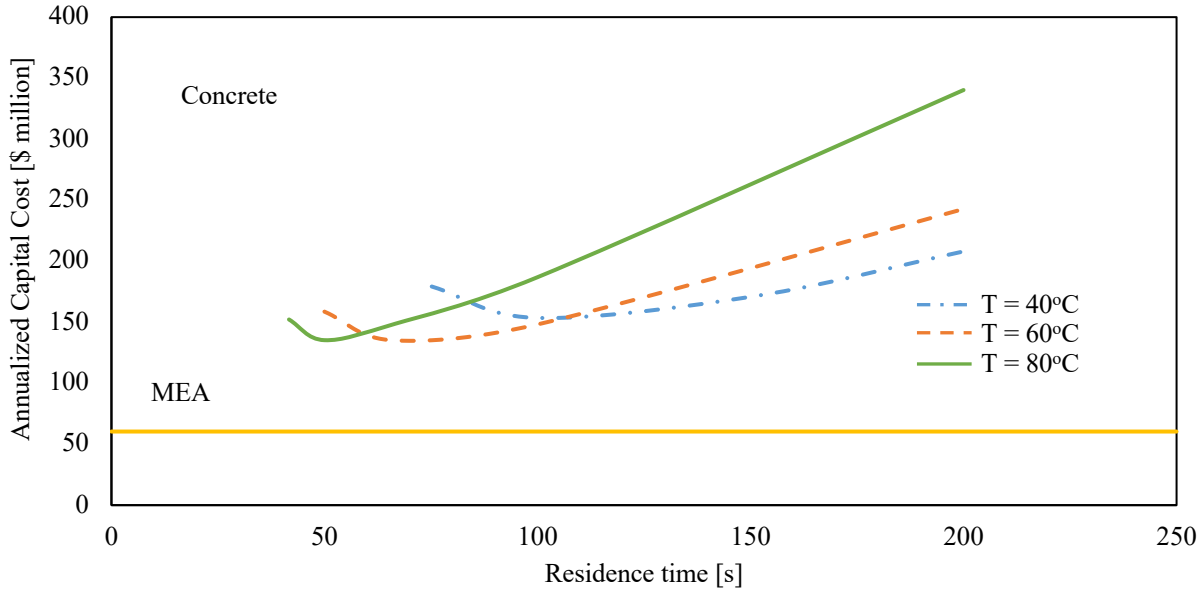

Figure 12. Impact of residence time on EAOC for different initial bed temperatures with concrete as the material of construction for the beds.

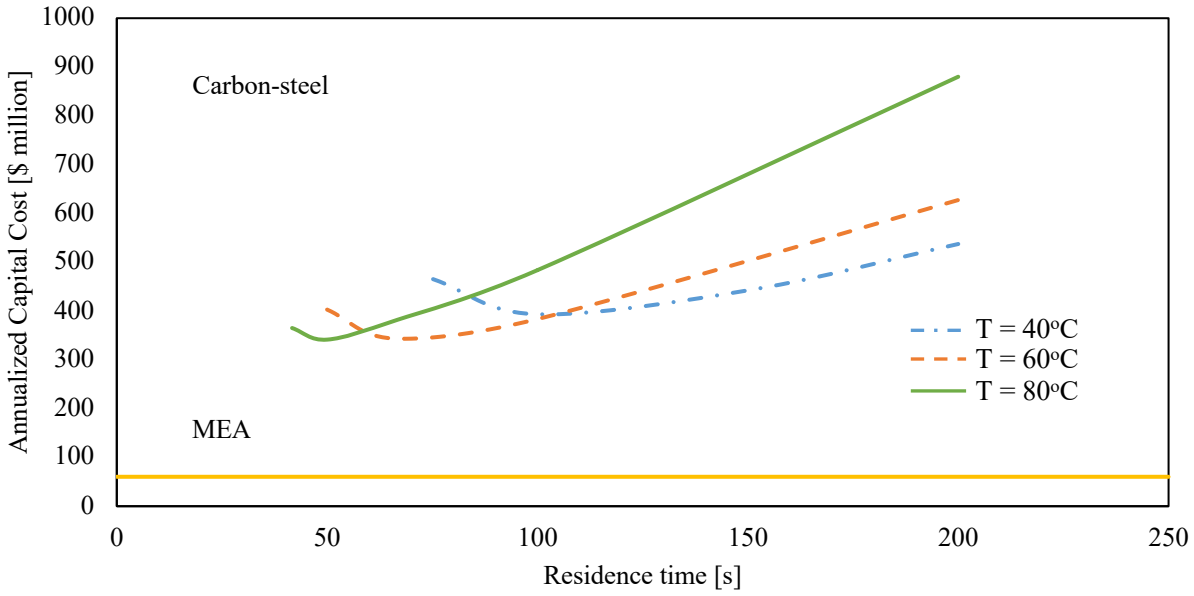

Figure 13. Impact of the residence time on the annualized capital cost for various initial bed temperatures with carbon steel as the material of construction for the beds.

The optimum EAOC value depends on the amount of heat recovery that can be achieved and also on the type of material used for contactor construction. As mentioned earlier, the sensible heat recovered from the liquid outlet stream in the case of MEA for 5°C temperature approach is about 80-90%. Thus, it is desired to compare the case when the heat recovery is similar to MEA. This study is conducted assuming a heat recovery of 85%, which is considered to be the best case scenario. It should be noted that such a high extent of heat recovery can be very difficult to achieve, if not impossible, for fixed beds and the authors by no means indicate the feasibility of such high extent of heat recovery. Figures 14 and 15 show the EAOC for varying residence time at different initial bed temperatures for concrete and carbon steel as the material of construction, respectively. The EAOC for the MEA system is also shown in both the figures. In Figure 14, it can be observed that the optimal initial bed temperature is 60°C and the minimum EAOC for the MECS system with the concrete contactor is approximately 1.8 times higher than the MEA technology. Figure 15 shows that the minimum EAOC that corresponds to the initial bed temperature of 60°C is approximately 2.7 times that for the MEA technology. The EOAC values for both concrete and carbon-steel with a range of heat recovery percentages are listed in the supporting information.

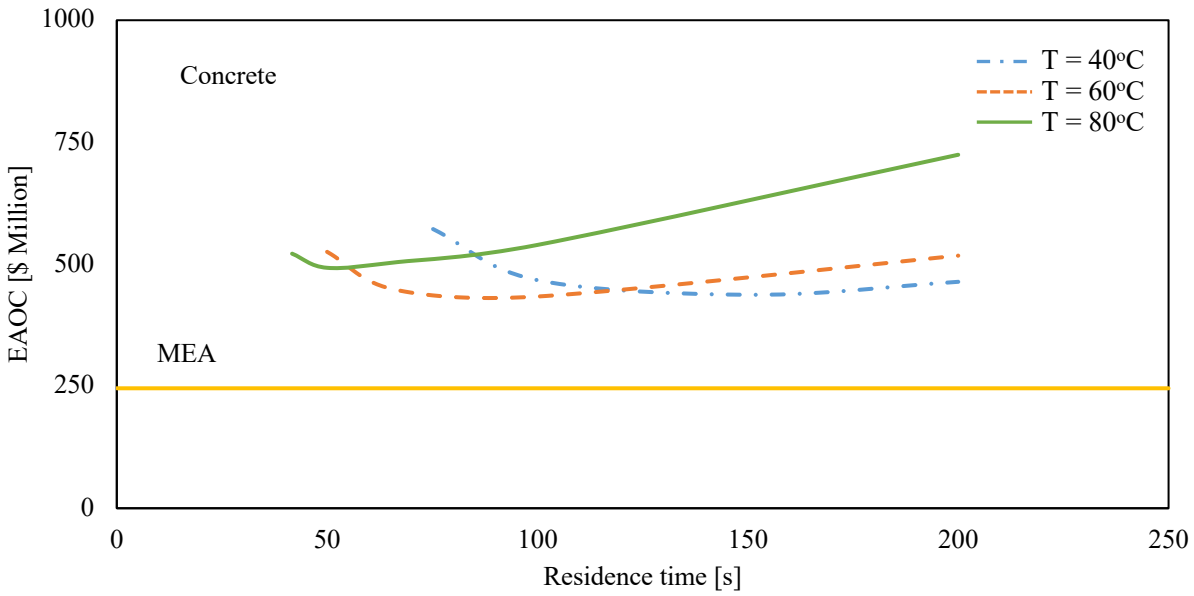

Figure 14. Impact of the residence time on EAOC for 85% heat recovery for concrete contactors at various initial bed temperatures.

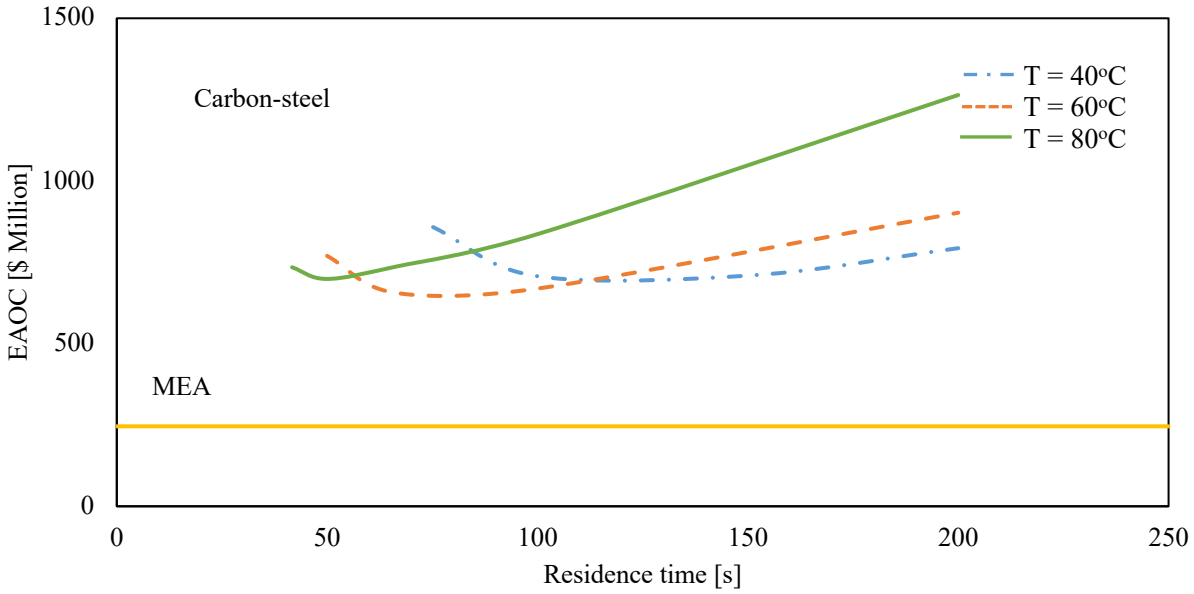

Figure 15. Impact of the residence time on EAOC for 85% heat recovery for carbon steel contactors at various initial bed temperatures.

6.5.2. Uncertainty analysis. Since there is no capital cost data available for these systems from real life, there can be high uncertainty in the capital cost estimates. EAOC values with +50% uncertainty in the carbon steel contactor cost and -50% uncertainty in the concrete contactor cost are evaluated since they serve as upper and lower bounds, respectively. Figures 16 and 17 show the EAOC for 60% and 85% heat recovery, respectively, when the initial bed temperature is 60°C. It is observed that the uncertainty in the capital cost estimation and the extent of heat recovery can have considerable impact on the optimum EOAC value. Obviously, -50% uncertainty in the concrete contactor cost leads to the minimum EAOC for both 60% and 85% heat recovery. Even with consideration of uncertainty, the minimum EAOC for 60% heat recovery is about 2.5 times higher than the MEA technology whereas for 85% heat recovery the minimum EAOC value is 1.5 times of the MEA technology. However, as noted earlier, achieving such a high extent of heat recovery in a fixed bed system would be difficult. The 10X rate did not offer much improvement in the EOAC values as shown in Figures 16 and 17.

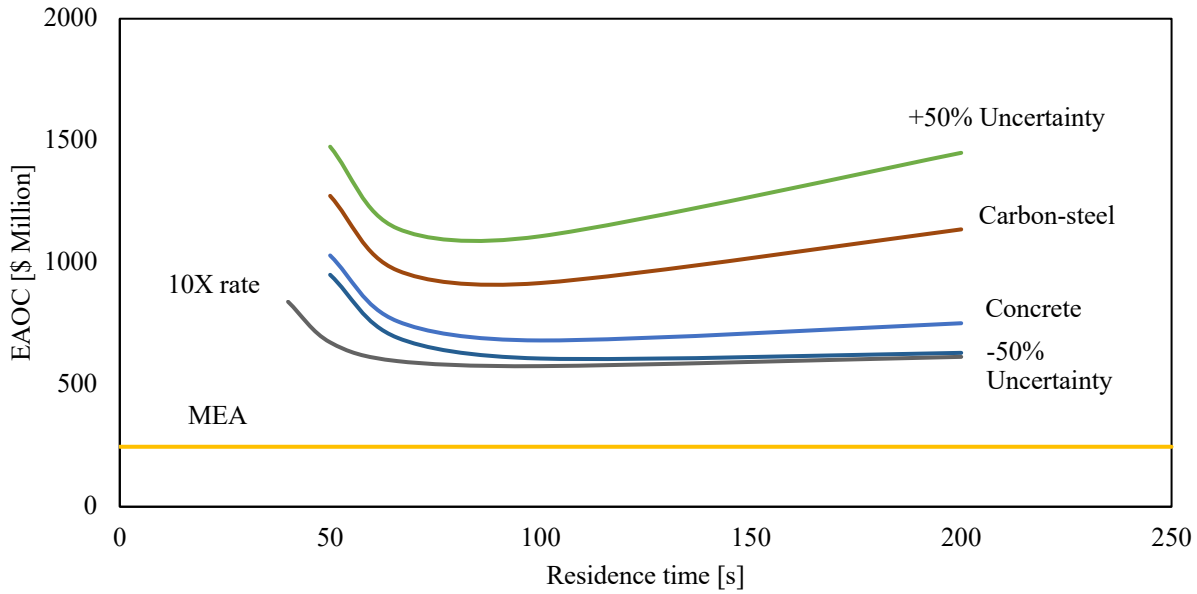

Figure 16. Impact of residence time on EAOC by considering uncertainty in the capital cost (60% heat recovery) for the initial bed temperature at 60°C.

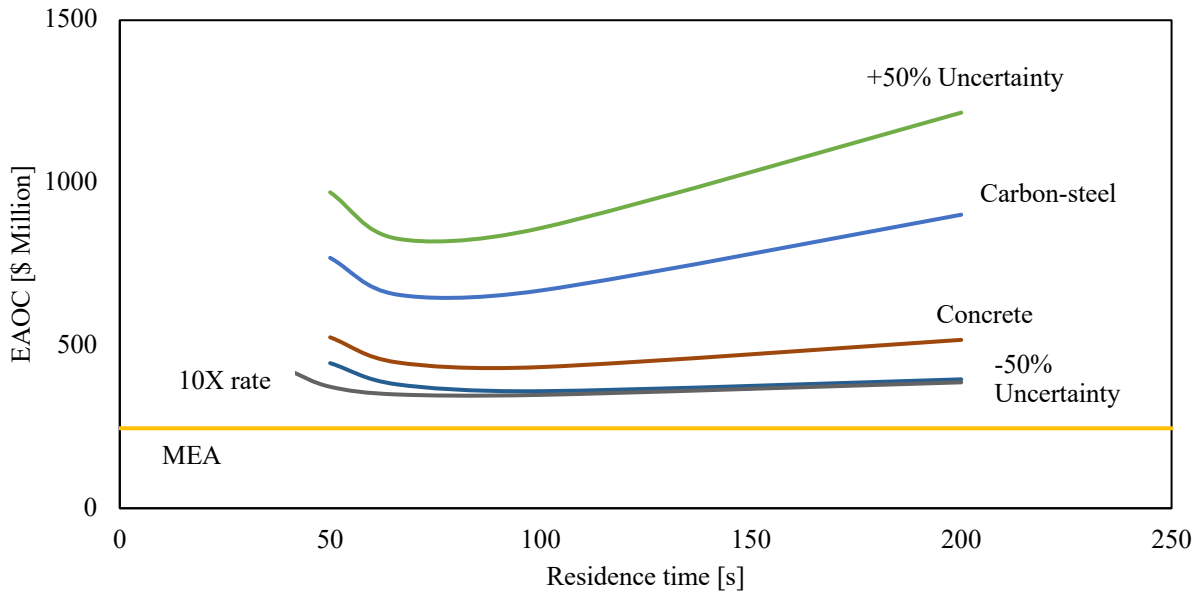

Figure 17. Impact of residence time on EAOC by considering uncertainty in the capital cost (85% heat recovery) for the initial bed temperature at 60ºC.

7. CONCLUSIONS

A rigorous model of a single capsule containing the sodium carbonate solution is developed. Model parameters and initial solvent concentration are estimated using the experimental CO_2 absorption data. A detailed model of a fixed bed of these capsules with an embedded heat exchanger is developed and used to simulate absorption-desorption cycles. The sensitivity of the fixed bed with respect to flue gas residence time and absorber initial bed temperature is analyzed. One key observation is that the number of beds required is large, regardless of residence time. Thus, a carbon capture installation unit using fixed beds of MECS can be cumbersome in size if carbonate solution is the solvent. Obviously the number of beds can be reduced by increasing the bed diameter. But, beds of very large diameter can lead to issues related to non-uniform gas distribution. Therefore, experimental studies are needed to determine the largest practical diameter of the bed. The results of this study also demonstrate that heat recovery is necessary to keep the energy penalty of this system low. However, heat recovery could prove challenging in a real fixed bed system due to the gradients and transient temperature profiles in these beds. The modeling results also show that there's an optimum flue gas residence time to keep the number of beds at a minimum. The minimum number of beds required is around 90, each bed with a volume of 1767 m^3, for a flue gas residence time of 100 s. A techno-economic analysis is performed where the equivalent annual operating cost (EAOC) is calculated for two different materials of construction- concrete, and carbon steel. The optimum EAOC depends on the material of construction, initial bed temperature, extent of heat recovery and residence time.

With 85% heat recovery and a concrete contactor, the minimum EAOC is approximately 1.8 times higher than the EAOC of a conventional MEA absorber

When uncertainty is factored into the TEA, the minimum EAOC is still 1.5 times higher than the EAOC for a MEA absorber. The system size and cost results of this study demonstrate that a fixed bed configuration of capsules filled with carbonate solution isn't competitive with a conventional MEA absorber for carbon capture from a power plant. However, this modeling study is based on a very slow-acting core solvent (20wt% sodium carbonate solution) serves as a starting point for MECS based CO_2 capture. Changing the core solvent in the capsules (e.g. using a higher carbonate concentration, an ionic liquid), would likely result in more competitive system sizes and costs. The model developed here provides a useful tool for modeling the performance and cost of fixed bed temperature swing absorption systems for encapsulated solvents.

ACKNOWLEDGEMENTS

This research was conducted through the Carbon Capture Simulation for Industry Impact ($CCSI^2$), funded through the U.S. DOE Office of Fossil Energy by the Los Alamos National Laboratory through contract# 379419. The authors also gratefully acknowledge the help from Dr. Gary Rochelle from University of Texas, Austin for calculating the cost of the concrete contactors.

NOMENCLATURE

A	Area [m^2]
a_e	Surface area to volume ratio [1/m]
C_T	Total concentration [kmol/m^3]
C	Concentration of species in the shell [kmol/m^3]
C^*	Free species concentration in the liquid core [kmol/m^3]
C_p	Specific heat capacity [kJ/kgK]
d	Diameter [m]
D	Diffusivity of species in the shell [m^2/s]
ϵ_{bed}	Porosity of the bed
E	Enhancement factor
H	Enthalpy [kJ/kmol]
h	Heat transfer coefficient [kW/m^2K]
$\overline{H}$	Partial molar enthalpy [kJ/kmol]
He_{CO_2}	Henrys constant of CO_2 [kPa m^3/kmol]
Ha	Hatta Number
k	Mass transfer coefficient [m/s]
K	Thermal conductivity [kW/mK]
K_{eq}	Equilibrium constant
k_1	Rate constant for the kinetically controlling reaction
N	Molar flux of the species at the shell surface [kmol/m^2s]
P	Pressure [kPa]
R	Radius [m]
T	Temperature [K]
u	Superficial velocity [m/s]
V_R	Volume of the reaction chamber [m^3]
μ	Viscosity [kmol/ms]
ρ	Density [kmol/m^3]
ϕ	Fugacity of the species
γ	Activity coefficient of the species
$f_{H_2O}^L$	Vapor pressure of water
x	Mole fraction of species

Subscript

i	Species
G	Gas phase
c, core	Core part of the capsule
cap	Capsule
$shell$	Shell part of the capsule
$surf$	Surface of the capsule
L	Liquid
hxw	Heat exchanger wall
gs	Gas to solid interaction
$hxwG$	Heat exchanger wall to gas interaction

ASSOCIATED CONTENT

Supporting information

Fixed bed model correlations and EAOC values for different operating ranges and materials in a tabular form.

REFERENCES

1. Knuutila, H., Juliussen, O., Svendsen, H.F., "Kinetics of the reaction of carbon dioxide with aqueous sodium and potassium carbonate solutions", Chemical Engineering Science, 65, 2010.
2. Knuutila, H., Juliussen, O., Svendsen, H.F., "Density and N_2O solubility of sodium and potassium carbonate solutions in the temperature range 25ºC to 80ºC", Chemical Engineering Science, 65, 2010.
3. https://www.eia.gov/outlooks/aeo/pdf/aeo2019.pdf
4. Knipe, J., Chavez, K., Hornbostel, K., Worthington, M., Nguyen, D., Ye, C., Bourcier, W., Baker, S., Brennecke, J., Stolaroff, J. Evaluating the performance of micro-encapsulated CO_2 sorbents during CO_2 absorption and regeneration cycling. Environmental science & technology. doi: 10.1021/acs.est.8b06442, 2019.
5. Knuutila, H., Hessen, E.T., Kim, I., ToreHaug-Warberg., Svendsen, H.F., "Vapor–liquid equilibrium in the sodium carbonate–sodium bicarbonate–water–CO_2 system", Chemical Engineering Science, 65, 2010.
6. Astarita G., Savage, D. W., Longo, J. M., "Promotion of Mass Transfer in Carbonate Solutions", Chemical Engineering Science, 36, 581, 1981.
7. Edwards, T., Maurer, G., Newman, J., Prausnitz, J., "Vapor-Liquid equilibria in multicomponent aqueous solutions of volatile weak electrolytes", AICHE Journal 24 (6), 966-976, 1978.
8. Pinsent B.R., Pearson L., Roughton F.J.W., "The Kinetics of Combination of Carbon Dioxide with Hydroxide Ions", Trans. Faraday Soc., 52, 1512-1520, 1956.
9. Robert L Berg, Cecil E Vanderzee, Thermodynamics of carbon dioxide and carbonic acid: (a) the standard enthalpies of solution of $Na_2CO_3(s)$, $NaHCO_3(s)$, and $CO_2(g)$ in water at 298.15 K; (b) the standard enthalpies of formation, standard Gibbs energies of formation, and standard entropies of $CO_2(aq)$, $HCO_3^-(aq)$, $CO_3^{2-}(aq)$, $NaHCO_3(s)$, $Na_2CO_3(s)$, $Na_2CO_3 \cdot H_2O(s)$, and $Na_2CO_3 \cdot 10H_2O(s)$, The Journal of Chemical Thermodynamics, Volume 10, Issue 12, 1978.
10. Gao,S, Guo,D, Jin,H, Sheng Li, Wang,J, and Wang,S., Potassium carbonate slurry-based CO_2 capture Technology, Energy & Fuels 2015 29 (10), 6656-6663.

11. Knuutila, H., Svendsen, H.F., Anttilla M., " CO_2 capture from coal-fired power plants based on sodium carbonate slurry; a systems feasibility and sensitivity study", International journal of greenhouse gas control, 3, 143-151, 2009.
12. Cussler, E.L., Diffusion: Mass Transfer in Fluid Systems. 2nd ed. 1997: New York: Cambridge University Press.
13. Kumar, A. and S. Hartland. "Correlations for prediction of mass transfer coefficients in single drop systems and liquid–liquid extraction columns." Chemical Engineering Research and Design 1999, 77(5): 372-384.
14. Vericella, J. J., Baker, S. E., Stolaroff, J. K., Duoss, E. B., Hardin, J. O., Lewicki J., Glogowski, E., Floyd W. C., Valdez, C. A., Smith, W. L., Satcher Jr J. H., Bourcier, W. L.., Spadaccini, C. M., Lewis, J. A., and Aines, R.D., Encapsulated liquid sorbents for carbon dioxide capture. Nature Communications, 6:6124, 1-7, 2015.
15. Reynolds, A. J., Verheyen, T. V., Adeloju, S. B., Meuleman, E. & Feron, P. Towards commercial scale post combustion capture of CO_2 with monoethanolamine solvent: key considerations for solvent management and environmental impacts. Environ. Sci. Technol. 46, 3643–3654, 2012.
16. Benson, H.E., Field, J.H., Jimeson, R.M., CO_2 absorption employing hot potassium carbonate solutions. Chem. Eng. Prog. 50, 10, 1954.
17. Pohorecki,R., Kucharski,E .Desorption with chemical reaction in the system CO_2-aqueous solution of potassium carbonate. Chem.Eng.J. 46, 1–7, 1991.
18. Savage, D., Astarita, G., Shriram, J., Chemical absorption and desorption of carbon dioxide from hot carbonate solutions. Chem. Eng. Sci., 35, 1513–1522, 1980.
19. Bonjour, J, Chalfen,J.B, and Meunier, F, Temperature Swing Adsorption Process with Indirect Cooling and Heating. Industrial & Engineering Chemistry Research, *41* (23), 5802-5811, 2002.
20. Clausse, M., Merel, J., Numerical parametric study on CO_2 capture by indirect thermal swing adsorption. International Journal of Greenhouse Gas Control, 5, 1206-1213, 2011.
21. G. Salazar Duarte., B. Schürer., C. Voss., and D. Bathen, Modeling and simulation of a tube bundle adsorber for the capture of CO_2 from flue gases, Chem.Ing.Tech. 88 3, S. 336-345, 2016.
22. B. Metz, O. Davidson, H. de Coninck, M. Loos, L. Meyer, Eds., Special Report on Carbon Dioxide Capture and Storage (Cambridge Univ. Press, Cambridge, 2005).
23. Nielsen, C. J., Herrmann, H. & Weller, C. Atmospheric chemistry and environmental impact of the use of amines in carbon capture and storage (CCS). Chem. Soc. Rev. 41, 6684–6704, 2012.
24. Stolaroff, J. K.; Ye, C.; Oakdale, J. S.; Baker, S. E.; Smith, W. L.; Nguyen, D. T.; Spadaccini, C. M. & Aines, R. D., Microencapsulation of advanced solvents for carbon capture. Faraday Discussions. DOI: 10.1039/c6fd00049e (2016).

25. Nathalie J.M.C. Penders-Van Elk, E. S.Hamborg, Patrick J.G.Huttenhuis, S.Fradette, J.A.Carley, G.F.Versteeg, " Kinetics of absorption of carbon dioxide in aqueous amine and carbonate solutions with carbonic anhydrase", International Journal of Greenhouse Gas Control, 12, 259-268, 2013.
26. Kohl, A.L., Nielsen.R, "Gas Purification. 5th ed., Gulf Professional Publishing. 1997.
27. Watson, J.M. & Baron, Mark. The behaviour of water in poly (dimethylsiloxane). Journal of Membrane Science, 110. 47-57. 10.1016/0376-7388(95)00229-4, 1996.
28. Turton, R., Shaeiwitz, J.A., Bhattacharyya, D., Whiting, W.B., 2018. Analysis, Synthesis, and Design of Chemical Processes, 5th ed. Prentice Hall.
29. Fout.T, Cost and Performance Baseline for Fossil Energy Plants Volume 1. 2015. DOI: DOE/NETL-2015/1723.
30. Anggit Raksajati, Minh T. Ho, and Dianne E. Wiley, Techno-economic Evaluation of CO_2 Capture from Flue Gases Using Encapsulated Solvent, Industrial & Engineering Chemistry Research. 56 (6), 1604-1620, 2017.
31. Justin R. Finn., Janine E. Galvin., Modeling and simulation of CO_2 capture using semipermeable elastic microcapsules, International Journal of Greenhouse Gas Control, ISSN: 1750-5836, Vol 74, 191-205, 2018.
32. K.Hornbostel, D.Nguyen, W.Bourcier, J.Knipe, M.Worthington, S.McCoy, J.Stolaroff, Packed and fluidized bed absorber modeling for carbon capture with micro-encapsulated sodium carbonate solution, Applied Energy, Vol 235, 1192-1204, 2019.
33. Rochelle, G. Private Communication with Dr. Gary Rochelle from University of Texas, Austin, 2018.
34. Stolaroff, J. Internal estimate by Dr. Stolaroff from Lawrence Livermore National Laboratory, Livermore, CA, 2018.

LIST OF FIGURES

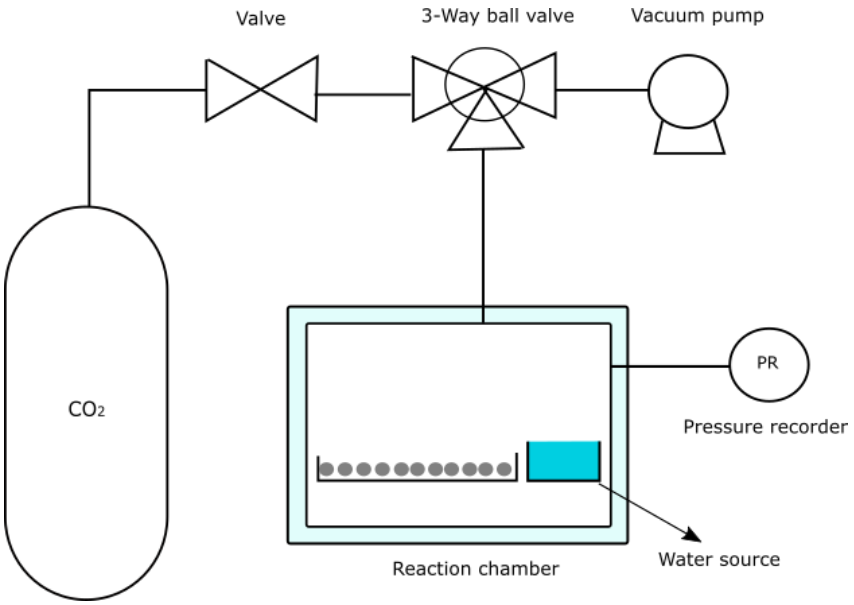

Figure 1. Experimental setup of CO_2 absorption using microcapsules filled with sodium carbonate.

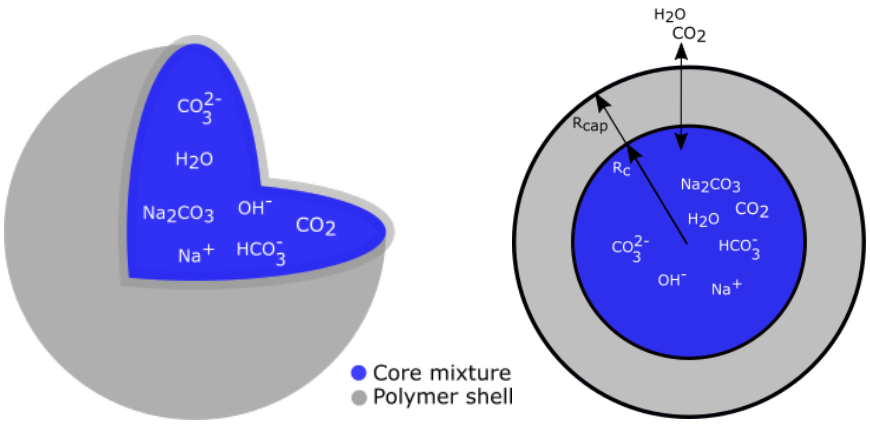

Figure 2. Schematic of microcapsule showing shell and core components.

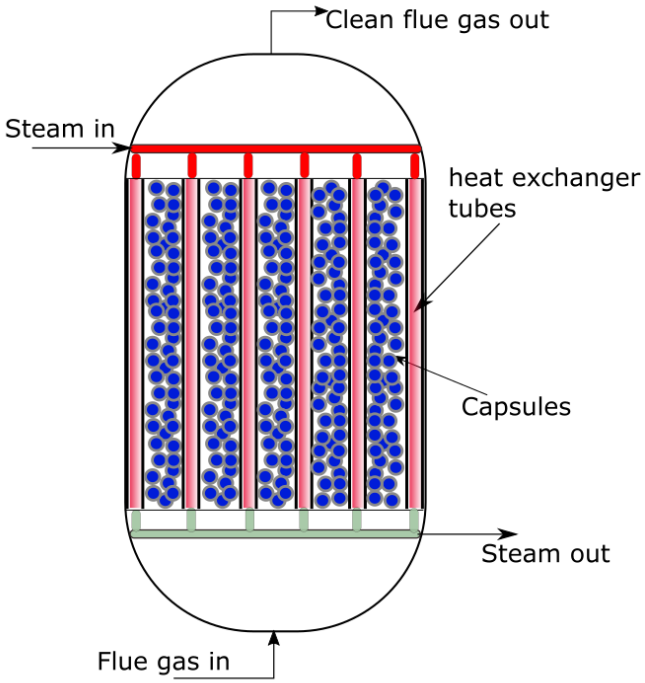

Figure 3. Schematic of fixed bed configuration for MECS showing capsules, heat exchanger tubes and flow directions.

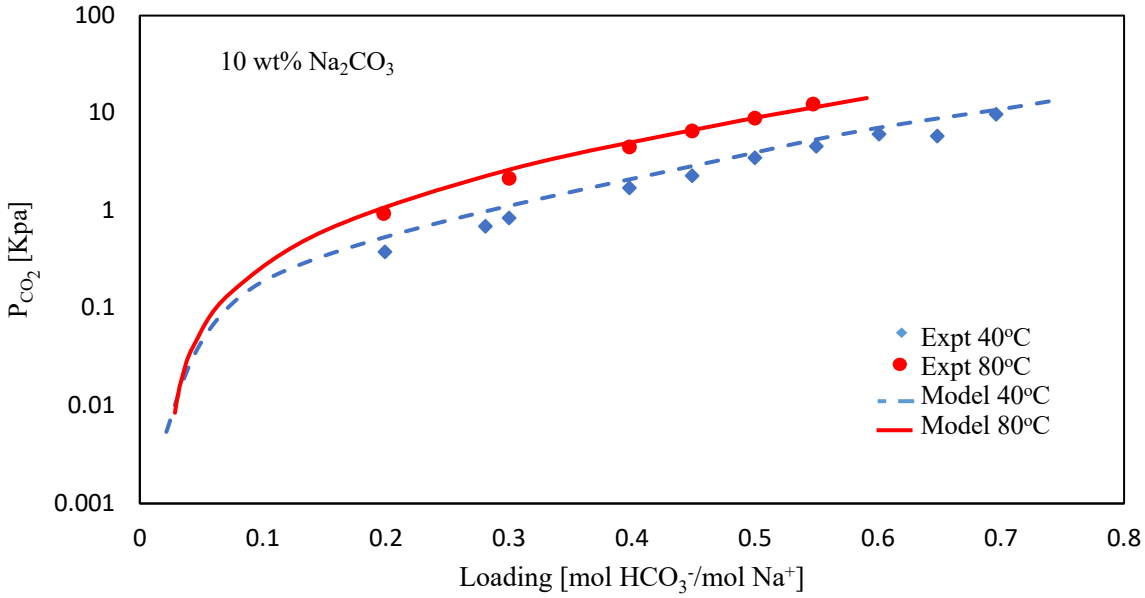

Figure 18 VLE model validation for 10 wt% Na_2CO_3 capsules.

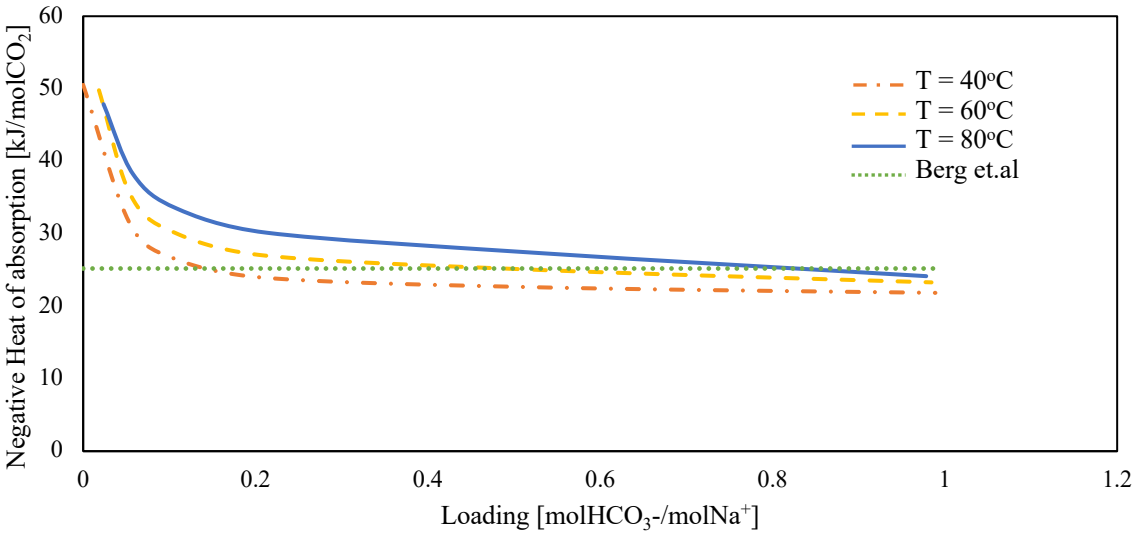

Figure 5. Heat of absorption for 10 wt% Na_2CO_3 solution.

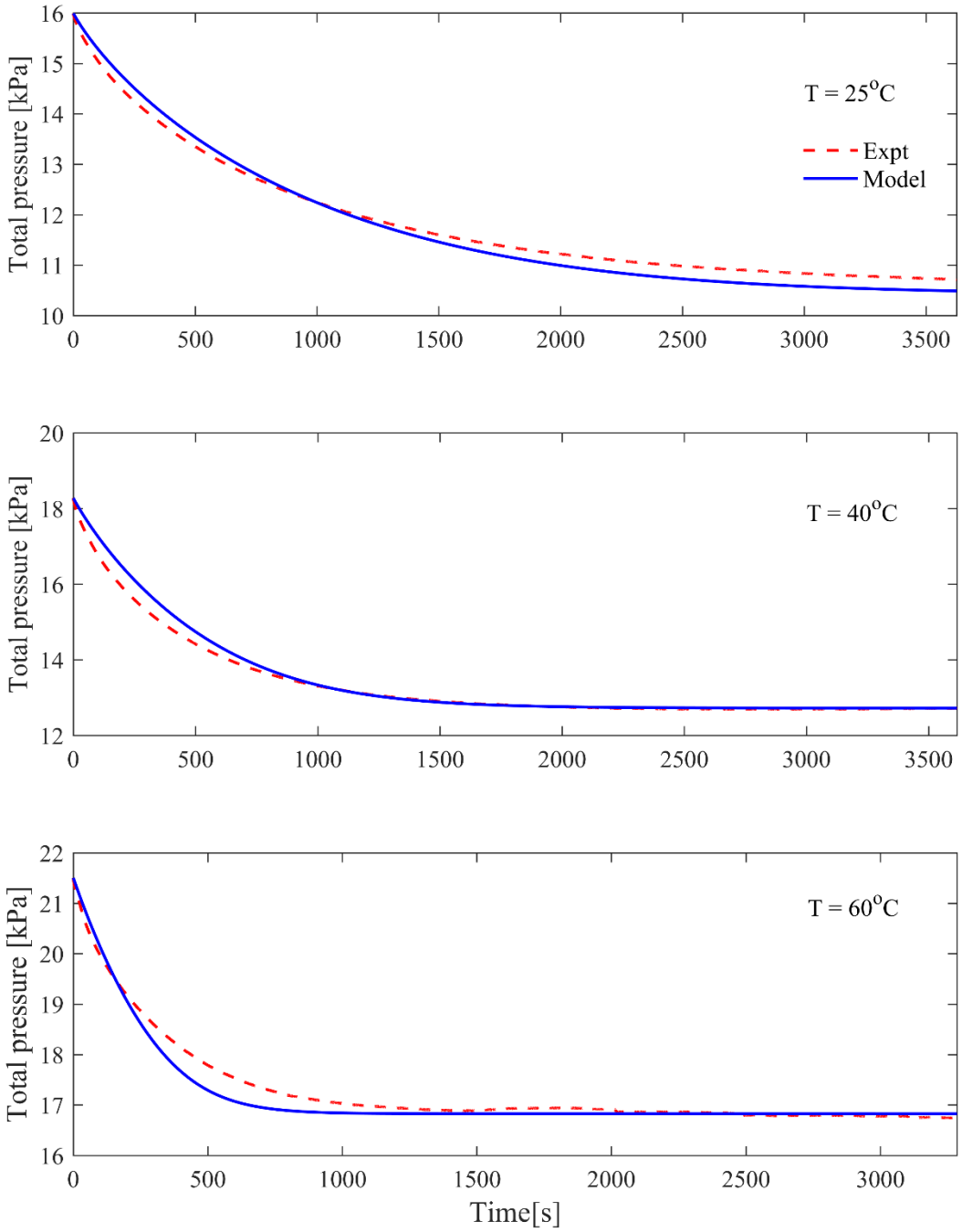

Figure 6. Comparison between the model results and the experimental data for the transients in the reactor chamber pressure at 25°C, 40°C, and 60°C.

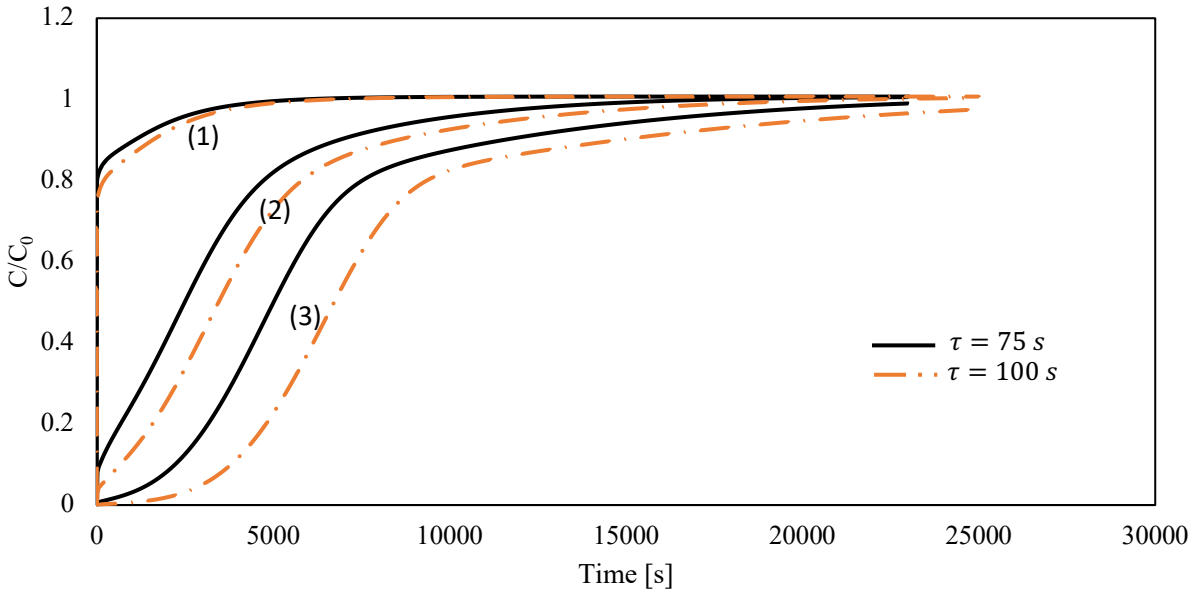

Figure 7. Breakthrough curve for different residence times at different locations: (1) entrance, (2) middle, (3) end of the bed.

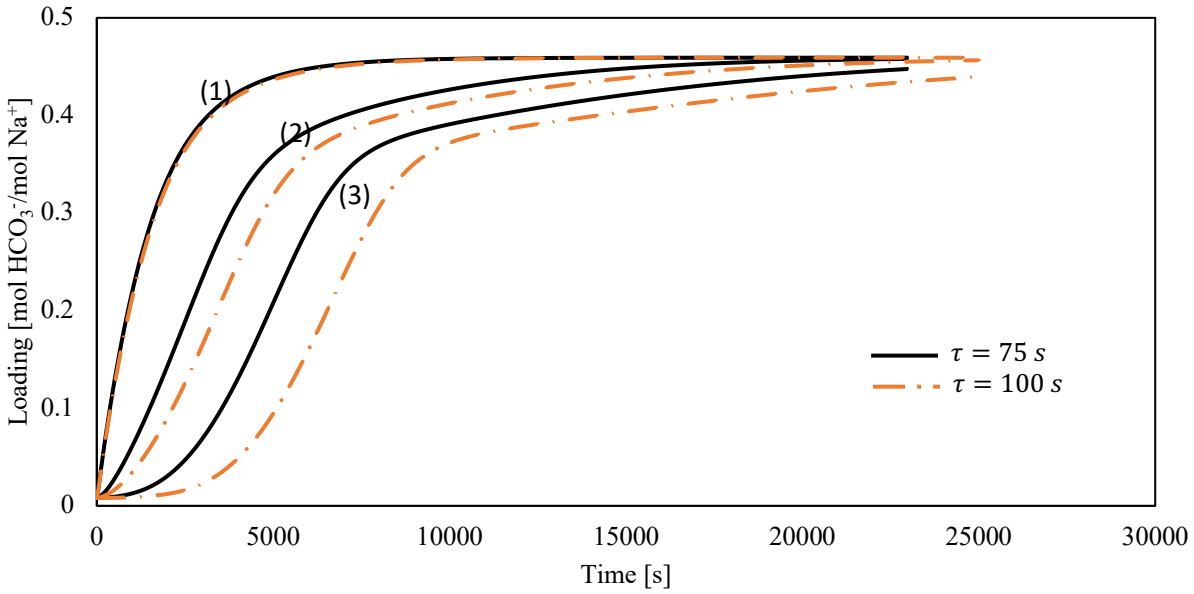

Figure 8. Loading comparison for different residence times at different locations: (1) entrance, (2) middle, (3) end of the bed.

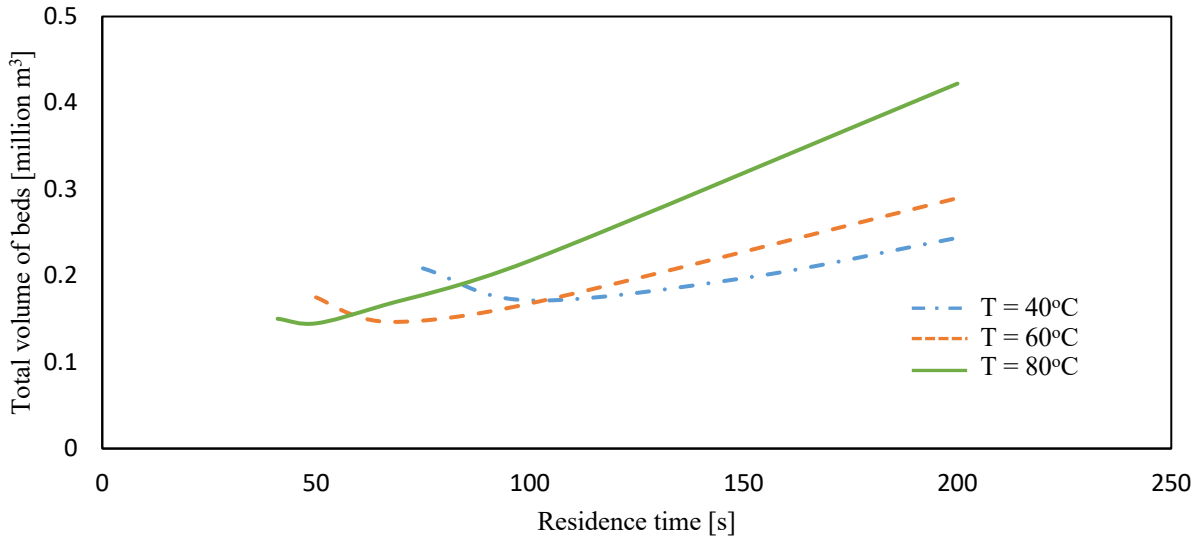

Figure 9. Impact of the residence time on the total volume of the beds at various initial bed temperatures.

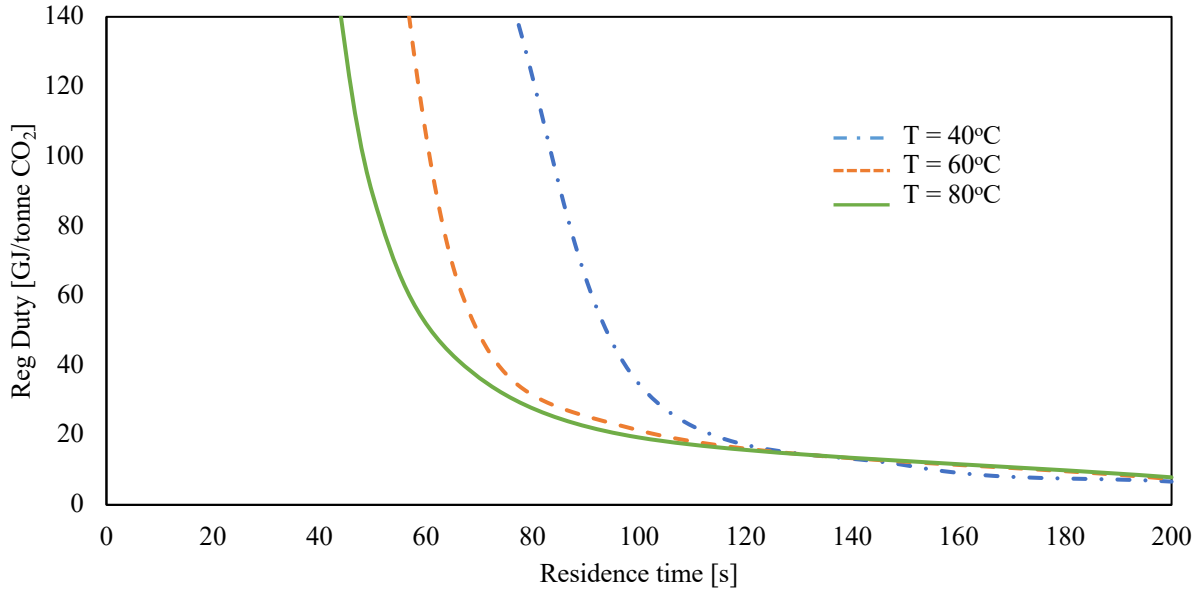

Figure 10. Impact of the residence time on the regeneration duty for various initial bed temperatures.

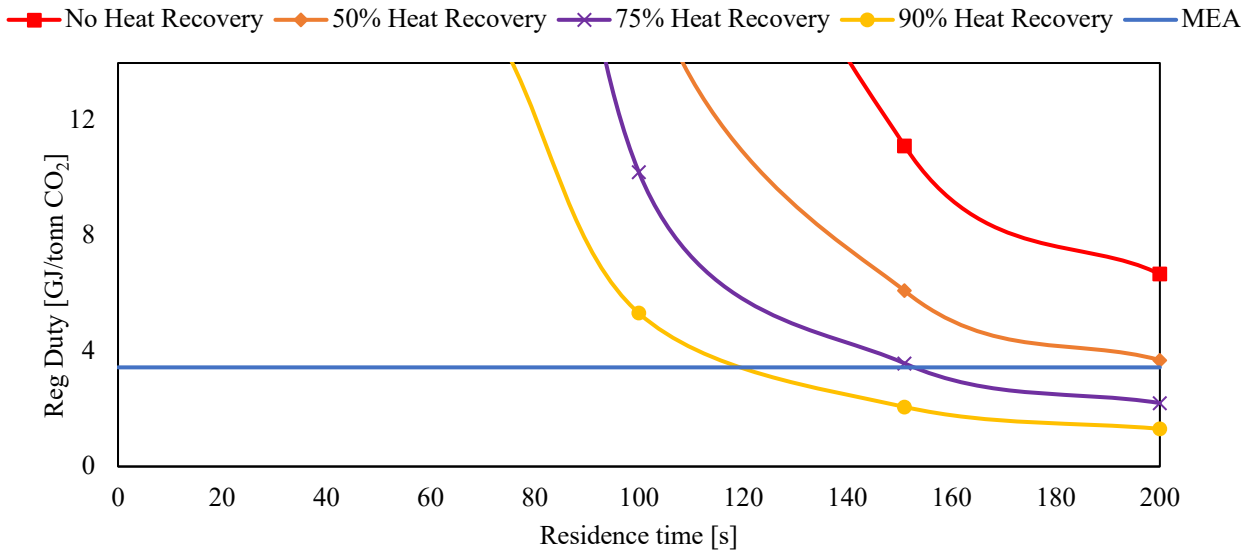

Figure 11. Impact of the residence time on regeneration duty for different extents of heat recovery.

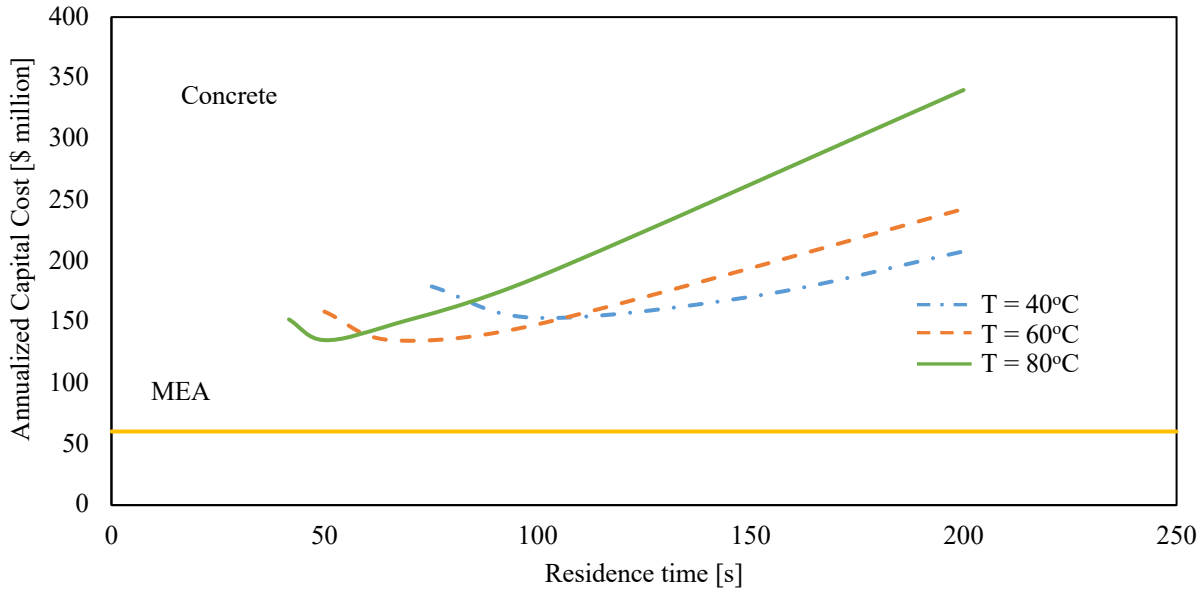

Figure 12. Impact of residence time on EAOC for different initial bed temperatures with concrete as the material of construction for the beds.

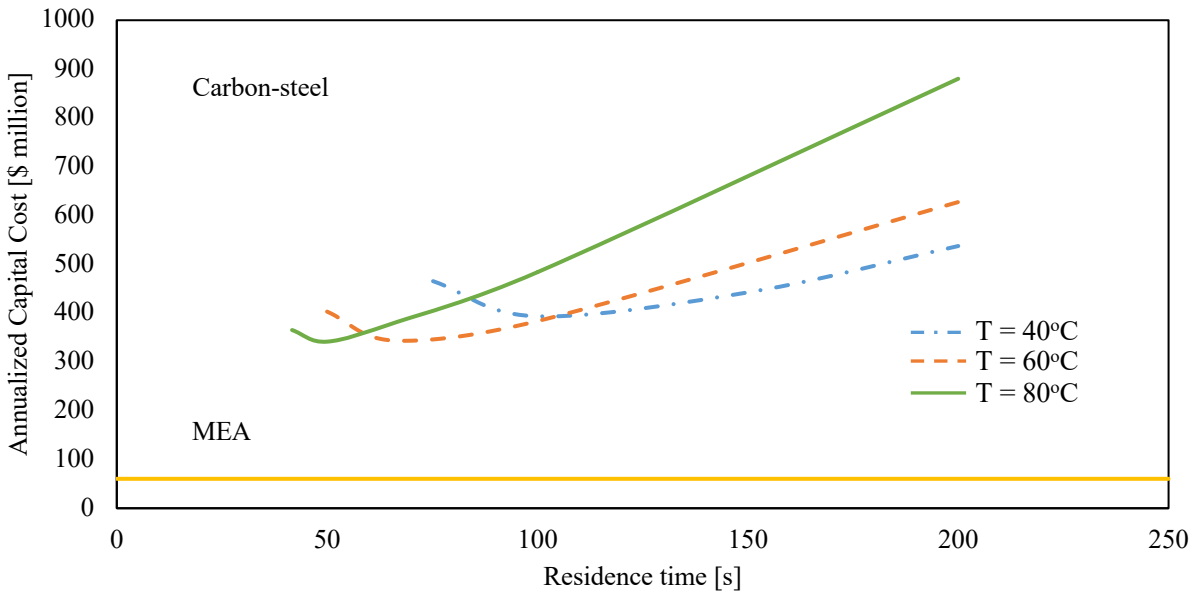

Figure 13. Impact of the residence time on the annualized capital cost for various initial bed temperatures with carbon steel as the material of construction for the beds.

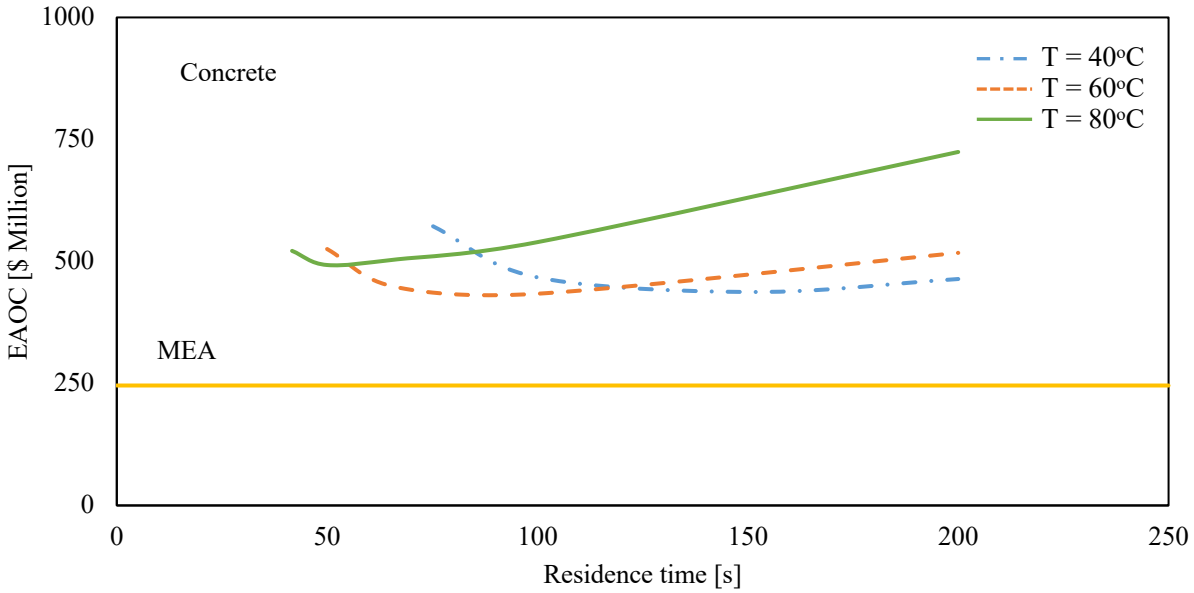

Figure 14. Impact of the residence time on EAOC for 85% heat recovery for concrete contactors at various initial bed temperatures.

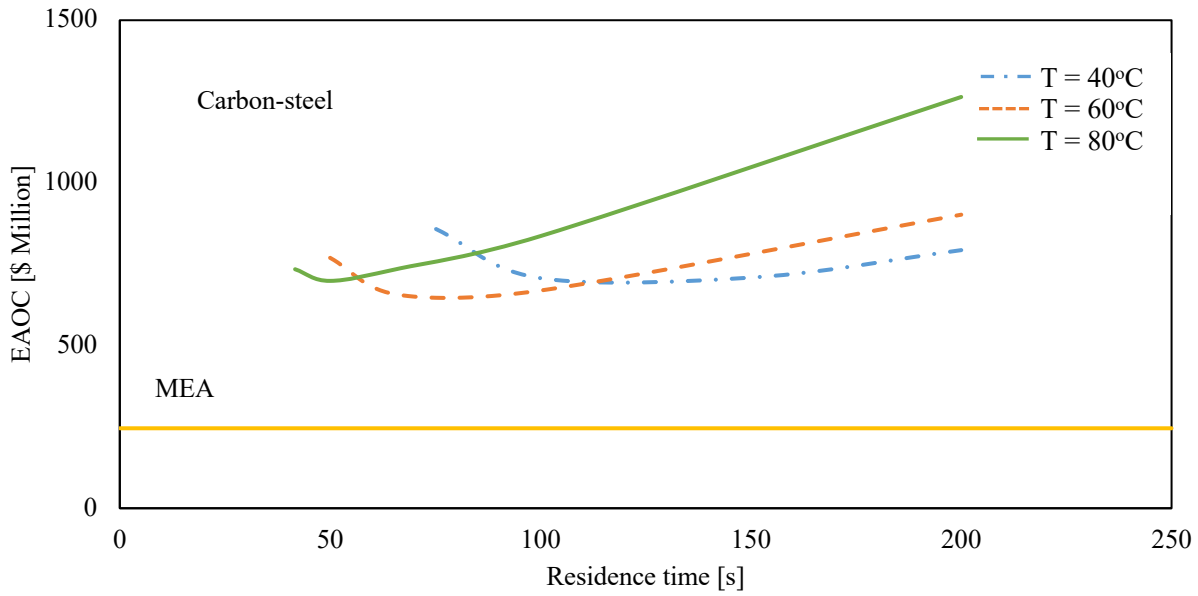

Figure 19. Impact of the residence time on EAOC for 85% heat recovery for carbon steel contactors at various initial bed temperatures.

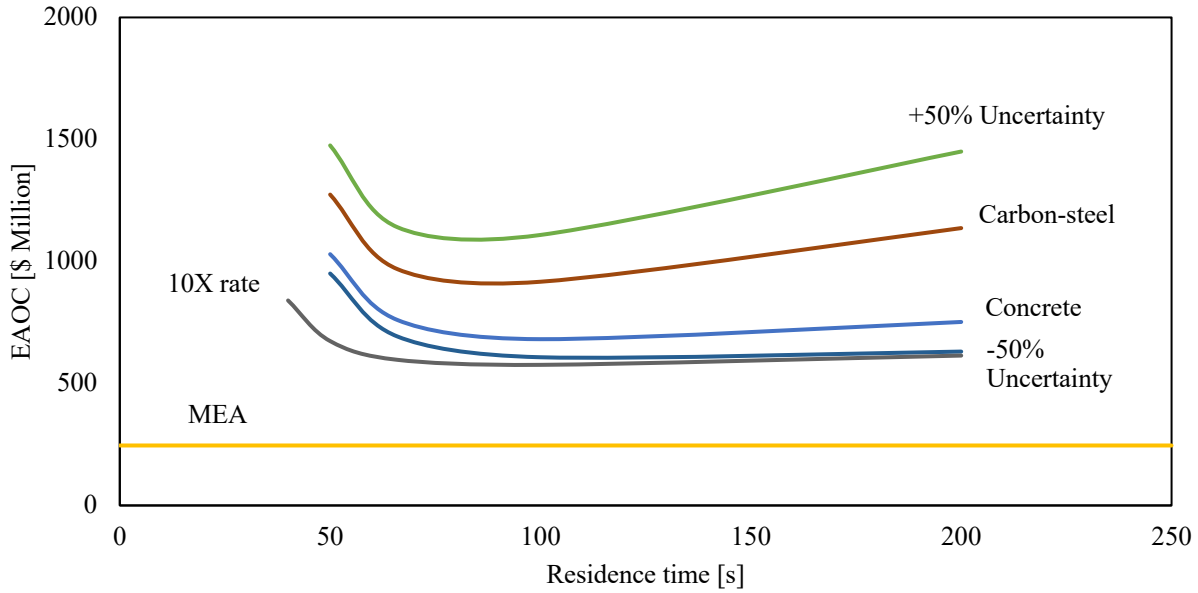

Figure 16. Impact of residence time on EAOC by considering uncertainty in the capital cost (60% heat recovery) for the initial bed temperature at 60°C.

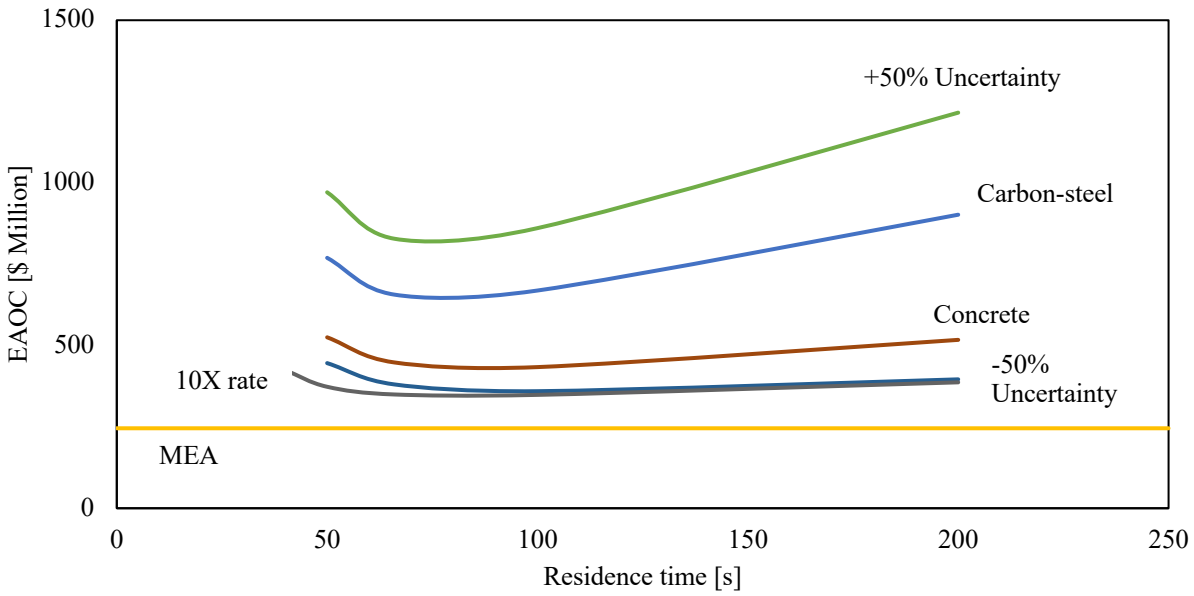

Figure 17. Impact of residence time on EAOC by considering uncertainty in the capital cost (85% heat recovery) for the initial bed temperature at 60°C.

LIST OF TABLES

Table 1. Dimensions of the microcapsules and volume of the chamber

Variable Name	Symbol	Value	Units
Capsule Radius	R_{cap}	3e-4	m
Core Radius	R_c	2.63e-4	m
Reaction chamber Volume	V_R	4.5e-5	m^3

Table 2. Unit prices used in the capital cost estimation of concrete and capsules

	Cost	Basis	Source
Concrete	2174 ($/$m^2$)	Internal wall to floor area	(Rochelle, 2018)
Capsule	0.0593 ($/kg)	Mass of capsules	(Stolaroff, 2018)

Table 3. Estimated model parameters and reconciled variables

Temperature	Parameter/Variable	Estimated/ reconciled value	Lower bound	Upper bound	Units	Std. deviation	Initial value
	C_1	2.153e-8	1e-8	1e-5	[m^2/s]	4.6e-10	2.5e-8
	C_2	1106	1000	2500	[K]	6.7	1200
25°C	Solvent	7.8	5	12	wt%	0.003	10
40°C	concentration	7.6	5	12	wt%	0.002	10
60°C		6.2	5	12	wt%	0.002	10

Table 4. Key variables in the fixed bed operation.

Absorption Stage	Value	UOM
Length of the bed	10	m
Diameter of the bed	15	m
Outlet gas pressure	1.0	bar
Solvent concentration	20	wt%
Desorption Stage		
Inlet steam temperature	130	°C
Steam residence time	100	s
Specific area for indirect heating	117	m^2/m^3
Average loading at the end of cycle	0.1	mol HCO_3^-/mol Na^+

Table 5. Impact of residence time on the number of beds and cycle times.

Residence time (τ) (s)	Breakthrough time (t_b) (s)	Desorption time (s)	Absorption beds	Total beds in the cycle
75	922	3425	25	118
100	2765	4223	38	97
150	6723	4495	67	112
200	10362	4518	96	138

Table 6. Key parameters showing energy and volume requirements for MECS in a fixed bed configuration.

	Normal rate		10 x normal rate	
Variable	$\tau = 75\ s$	$\tau = 100\ s$	$\tau = 75\ s$	$\tau = 100\ s$
Absorption time	922	2765	2211	4053
Desorption time	3425	4223	4292	4432
Total beds in the cycle	118	97	74	80
Total Volume (m^3)	208523	171413	130768	141371
Regeneration duty (GJ/tCO_2)	150	35	36	17